Inhibition of IRAK4 by microbial trimethylamine blunts metabolic inflammation and ameliorates glycemic control

Julien Chilloux[1,15], Francois Brial[2,15], Amandine Everard[3,15], David Smyth[4,15], Petros Andrikopoulos[1,5,15], Liyong Zhang[4], Hubert Plovier[3], Antonis Myridakis[1], Lesley Hoyles[1,6], José Maria Moreno-Navarrete[7], Jèssica Latorre Luque[7], Viviana Casagrande[8], Rosella Menghini[8], Blerina Ahmetaj-Shala[9], Christine Blancher[10], Laura Martinez-Gili[1], Selin Gencer[1], Jane F. Fearnside[10], Richard H. Barton[1], Ana Luisa Neves[1], Alice R. Rothwell[10], Christelle Gérard[2], Sophie Calderari[2], Mark J. Williamson[11], Julian E. Fuchs[10], Lata Govada[1], Claire L. Boulangé[1], Saroor Patel[1], James Scott[11], Mark Thursz[12], Naomi Chayen[1], Robert C. Glen[1,11], Nigel J. Gooderham[1], Jeremy K. Nicholson[1], Massimo Federici[8], José-Manuel Fernández-Real[7], Dominique Gauguier[1,2,10,16], Peter P. Liu[4,16], Patrice D. Cani[1,3,16], Marc-Emmanuel Dumas[1,5,13,14,16]¶

[1] Biomolecular Medicine, Division of Systems Medicine, Department of Metabolism, Digestion and Reproduction, Imperial College London, United Kingdom

[2] Sorbonne Universities, University Pierre & Marie Curie, University Paris Descartes, Sorbonne Paris Cité, INSERM UMR_S1138, Cordeliers Research Centre, 15 rue de l'Ecole de Médecine, 75006 Paris, France

[3] Université catholique de Louvain, Louvain Drug Research Institute, WELBIO (Walloon Excellence in Life sciences and BIOtechnology), Metabolism and Nutrition Research Group, 1200 Brussels, Belgium

[4] University of Ottawa Heart Institute, Ottawa ON K1Y 4W7, Canada

[5] Genomic & Environmental Medicine, National Heart & Lung Institute, Imperial College London, London, UK

[6]Department of Biosciences, Nottingham Trent University, Clifton Campus, Nottingham NG11 8NS, UK

[7]Department of Endocrinology, Diabetes and Nutrition and Department of Medicine, Hospital of Girona "Dr Josep Trueta", Faculty of Medicine, University of Girona and CIBERobn Pathophysiology of Obesity and Nutrition, Instituto de Salud Carlos III, Madrid, Spain

32 [8]Department of Systems Medicine, University of Rome Tor Vergata, Via Montpellier, Rome,
33 Italy
34 [9]Section of Vascular Biology, National Heart & Lung Institute, Imperial College London,
35 London, UK
36 [10] Wellcome Trust Centre for Human Genetics, Roosevelt Drive, University of Oxford, Oxford
37 OX3 7BN, UK, [8] National Heart and Lung Institute, Imperial College London, London, UK.
38 [11]Centre for Molecular Informatics, Department of Chemistry, University of Cambridge,
39 Lensfield Road, Cambridge CB2 1EW, UK
40 [12] Section of Hepatology & Gastroenterology, Division of Digestive Diseases, Department of
41 Metabolism, Digestion and Reproduction, Imperial College London, United Kingdom
42 [13]European Genomic Institute for Diabetes, U1283 INSERM, UMR8199 CNRS, Institut
43 Pasteur de Lille, Lille University Hospital, University of Lille, 1 place de Verdun, 59045 Lille,
44 France
45 [14]McGill Genome Innovation Centre, McGill University, 740 Avenue Dr. Penfield, Montréal,
46 Québec H3A 0G1, Canada
47 [15]These authors contributed equally and should be considered as co-first authors
48 [16]These authors contributed equally and should be considered as co-senior authors
49 ¶ correspondence should be addressed to M.-E.D.: m.dumas@imperial.ac.uk

Abstract

The global type 2 diabetes epidemic is a major health crisis and there is a critical need for innovative strategies to fight it. Although the microbiome plays important roles in the onset of insulin resistance (IR) and low-grade inflammation, the microbial compounds regulating these phenomena remain to be discovered. Here, we reveal that the microbiome inhibits a central kinase, eliciting immune and metabolic benefits. Through a series of *in vivo* experiments based on choline supplementation, blocking trimethylamine (TMA) production then administering TMA, we demonstrate that TMA decouples inflammation and IR from obesity in the context of high-fat diet (HFD) feeding. Through *in vitro* kinome screens, we reveal TMA specifically inhibits Interleukin-1 Receptor-associated Kinase 4 (IRAK4), a central kinase integrating signals from various toll-like receptors and cytokine receptors. TMA blunts TLR4 signalling in primary human hepatocytes and peripheral blood monocytic cells, and improves mouse survival after a lipopolysaccharide-induced septic shock. Consistent with this, genetic deletion and chemical inhibition of IRAK4 result in similar metabolic and immune improvements in HFD. In summary, TMA appears to be a key microbial compound inhibiting IRAK4 and mediating metabolic and immune effects with benefits upon HFD. Thereby we highlight the critical contribution of the microbial signalling metabolome in homeostatic regulation of host disease and the emerging role of the kinome in microbial–mammalian chemical crosstalk.

70 **Main**

71 Globally, diabetes affects 529 million individuals[1], claiming 1.6 million lives per year
72 according to the World Health Organization. Insulin resistance (IR) is a multifactorial
73 condition and now increasingly common due, among other factors, to the increase in
74 prevalence of a sedentary lifestyle, Western-style foods and obesity. IR is a risk factor for
75 developing type 2 diabetes and cardiovascular diseases[2]. One of the hallmarks of these
76 disorders is the early development of a chronic, systemic low-grade inflammation[3]. The
77 interaction between high-fat diet (HFD) feeding and the gut microbiome has a strong impact
78 on the onset of IR[4–6]: bacterial lipopolysaccharides (LPS) and dietary fats trigger low-grade
79 inflammation[2] through activation of *Toll*-like receptor 4 (TLR4), a process called metabolic
80 endotoxemia[7].

81 This is supported by a complex communication that occurs between the gut microbiota and
82 the innate immune system[8], with consequences on metabolic homeostasis[9]. Whilst some of
83 the functional signalling molecules mediating microbial–mammalian chemical crosstalk have
84 been characterized, a limited number of metabolite classes and their targets have been
85 identified (G protein-coupled[10] and nuclear receptors[11]). It is, however, hypothesized that
86 microbial metabolites potentially affect other pharmacological target classes such as
87 kinases[12]. In previous studies, we and others have identified a family of microbiome-
88 associated metabolites, methylamines, associated with IR, non-alcoholic fatty liver disease[13]
89 and atherosclerosis[14], but their mechanisms of action on mammalian hosts remain unclear.
90 Trimethylamine (TMA) is one of the most abundant microbial metabolites produced by the
91 gut microbiota. We first reported that TMA may be associated with IR[12]. TMA results from
92 microbial metabolism of dietary choline, carnitine and trimethylamine *N*-oxide (TMAO)[15–19]
93 before being absorbed and *N*-oxidized into TMAO by hepatic flavin-containing mono-
94 oxygenase 3 (FMO3)[20]. After initial reports associating TMAO with adverse cardiovascular
95 outcomes[13,16], it has since emerged that FMO3 inactivation was beneficial for several
96 metabolic outcomes[21–24], strongly suggesting that TMA and TMAO have distinct biological
97 roles.

98 Here, we decipher the role of TMA in the microbiota–host kinome chemical crosstalk in IR
99 through i) identification of gut-derived microbial metabolites associated with HFD-induced
100 impaired glucose tolerance (IGT), IR and obesity, ii) pharmacological target screening of
101 discriminant microbial metabolites, and iii) mechanistic validation of the pathophysiological

102 relevance of pharmacological interactions with *in vitro* and *in vivo* models. Using this
103 approach, we discovered a novel mechanism by which gut microbial TMA acts as an IRAK4
104 inhibitor and directly improves the host immune and metabolic tone.
105
106 **Lack of hepatic inflammation in HFD and the choline supplementation hypothesis.**
107 We initially carried out a longitudinal pathophysiological monitoring in a cohort of C57BL/6
108 mice (n=5 for HFD and n=6 for chow diet (CHD)) rapidly developing obesity and IGT when
109 fed a 65% kCal HFD with a range of macronutrient and micronutrient differences compared
110 to CHD (**Extended Data Fig. 1a-b, Fig. 1a** and **Supplementary Table 1**). Liver transcriptomics
111 (n=5-6 per diet group) identified 2,084 significantly (FDR < 0.1) differentially expressed
112 genes between CHD-fed and HFD-fed mice (**Extended Data Fig. 1c, Fig. 1b** and
113 **Supplementary Table 1**). Gene ontology and signalling pathway impact analyses (**Extended**
114 **Data Fig. 2, Supplementary Table 2-4**) demonstrated upregulation of protein processing in
115 the endoplasmic reticulum, whereas carbohydrate metabolism, circadian rhythm and AMPK
116 signalling were significantly inhibited, consistent with existing literature[25,26]. Surprisingly,
117 inflammation-associated pathways were not differentially affected: expression of genes
118 coding for acute phase serum amyloid A proteins *Saa1* and *Saa2* upregulated in response to
119 acute inflammation and associated with type 2 diabetes was reduced, whereas expression
120 of pro-inflammatory cytokines such as *Il6* and *Il1β* was not significant (**Fig. 1b** and
121 **Supplementary Table 4**). This is in contrast to established knowledge as low-grade
122 inflammation is one of the key features associated with IR[2,6] and HFD[27]. Beyond % of fat
123 content as a macronutrient, we therefore looked for variation in micronutrients and
124 microbial metabolites that may contribute to this phenotype by performing metabolic
125 profiling of the urinary metabolome of this mouse cohort (CHD and HFD, 4 time-points) by
126 ^{1}H-NMR spectroscopy followed by multivariate modelling. Our analysis showed diet is the
127 main factor influencing the metabolic profiles, followed by age (**Extended Data Fig. 1d**); the
128 model's goodness-of-prediction parameters being highly significant upon permutation
129 testing (**Extended Data Fig. 1e**). The metabolic signature of HFD-feeding compared to CHD
130 was mainly associated with TMA excretion (**Fig. 1c**), consistent with our previous reports
131 using this diet[13,28]. We used variance components analysis to decompose the contribution of
132 diet and age to the excretion of these three metabolites, showing that the HFD contribution
133 overwhelms the contribution of age (**Fig. 1d**). Since the HFD contains >15 g of choline per kg

134 of diet, we then investigated whether supplementation in this micronutrient could
135 modulate the metabolic and immune variation in response to HFD feeding.
136
137 **Choline supplementation corrects HFD-induced inflammation and IR.**
138 To test the effect of choline supplementation itself on glucose tolerance and IR in an HFD
139 context, we initiated a series of *in vivo* studies. We first fed C57BL/6 mice with a 65% kCal
140 HFD containing 2 g/kg or 17 g/kg of choline (i.e.: LC-HFD and HC-HFD, respectively; **Fig. 1e-**
141 **n**). To evaluate metabolic homeostasis, we performed glucose tolerance tests (GTTs), which
142 displayed a similar pattern with normalisation of cumulative glycemia on HC-HFD compared
143 to LC-HFD (**Fig. 1e-f**). Body weight (BW) was significantly increased in mice fed a LC-HFD
144 from weaning until 5 months of age compared to mice fed a chow diet and remarkably
145 compared to mice fed HC-HFD (**Fig. 1g**), which was not related to food intake (**Extended**
146 **Data Fig. 3a**). We then profiled circulating pro-inflammatory cytokines such as IL6, IL1β,
147 TNFα (**Fig. 1h-j**) and phosphorylation of NF-κB regulating their transcription (**Extended Data**
148 **Fig. 3b,c**), which was also suggestive of an improvement of HFD-induced inflammation by
149 choline supplementation.
150
151 **Targeted analysis of choline and methylamine pathways.**
152 To document the effect of choline supplementation on choline-related metabolic pathways,
153 we further refined our isotopic UPLC-MS/MS quantification[29,30] to evaluate plasma
154 concentrations of choline- and carnitine-derived metabolites leading to TMA and TMAO
155 (**Extended Data Fig. 3d,e**). An O-PLS-DA model significantly segregates the three treatment
156 groups at 5 months of age (i.e., 4 months of HFD) and highlights a choline supplementation
157 effect on the first predictive component (**Fig. 1k,l**). Quantifications all reflect an increase in
158 TMA and TMAO in the HC-HFD in line with choline supplementation (**Fig. 1m,n**). In
159 particular, the circulating TMA levels were similar in the CHD and the LC-HFD (0.38 µM in
160 CHD vs. 0.3 µM in LC-HFD) and were about 20 times lower than in the HC-HFD (5.9 µM).
161 These results depict an increased microbial conversion of choline into TMA in our HC-HFD,
162 an observation already made in a previous study[13]. These results suggest that TMA could
163 mediate the metabolic and immune benefits of choline supplementation.
164
165 **Baseline metabolic phenotyping after 2-month choline modulation in HFD.**

166 To further assess the impact of choline supplementation on metabolic homeostasis and low-
167 grade inflammation in HFD contexts, we performed a second experiment, feeding C57BL/6
168 mice a 60% kcal HFD with a time-frame comparable to the ones used in subsequent
169 experimental designs using osmotic minipumps for constant subcutaneous TMA delivery.
170 GTTs and weekly BWs showed a similar trend after 8 weeks of HFD-feeding (**Fig. 2a-d**).
171 Choline supplementation not only improved glucose tolerance (**Fig. 2a,b**) but also the
172 Matsuda index (**Fig. 2c**), a marker for IR derived from oral GTTs[31]. The normalisation of
173 insulin sensitivity was confirmed through insulin tolerance tests (ITTs) and insulin-induced
174 hepatic Akt phosphorylation assays (**Fig. 2e-h**). Notably, the normalisation of insulin-
175 induced hepatic AKT phosphorylation assays was primarily associated with a reduction of
176 basal level of P-AKT in HC HFD compared to LC HFD observed in saline condition
177 demonstrating the reduction of IR (**Fig. 2g**). Indeed, it has been previously demonstrated
178 that HFD increased the basal levels of P-AKT and this participates to IR[32]. We further
179 characterized that HFD feeding increased hepatic NF-κB phosphorylation compared to CHD,
180 which was normalised by choline supplementation (**Fig. 2i,j**), a pattern that was also
181 observed for expression of acute-phase proteins that are typically upregulated in response
182 to tissue inflammation[33] – *Saa1*, *Saa2* and *Saa3* (**Fig. 2k-m**).
183
184 **Chemical blockage of bacterial TMA biosynthesis and loss of metabolic benefits.**
185 To test whether the beneficial effects of choline supplementation are mediated by its
186 microbial product TMA, we sought to block bacterial TMA production in HC-HFD-fed mice
187 both non-specifically and specifically using a wide-spectrum antibiotics cocktail or 3,3-
188 dimethyl-1-butanol (DMB), inhibiting microbial TMA-lyase[34], respectively. We first
189 confirmed the functional blockage of TMA production in mice fed a HC-HFD, resulting in a
190 drastic drop in circulating and excreted TMA and TMAO following 1% DMB administration
191 (**Extended Data Fig. 4a-d**). In accordance with our hypothesis, both antibiotic and DMB
192 treatments abolished the effects of choline supplementation-induced improvements in HFD,
193 in particular for glucose tolerance, insulin sensitivity (as suggested by the Matsuda index,
194 **Fig. 3a-c**, **Extended Data Fig. 4e,f**) and hepatic insulin sensitivity as shown by the absence of
195 a beneficial effect of choline supplementation on insulin-induced Akt phosphorylation (**Fig.
196 3d-e**). The metabolic improvements associated with chemical TMA synthesis blockage were
197 not due to changes in BW gain (**Extended Data Fig. 4e**), thereby strongly suggesting that the

198 effects on glucose metabolism induced by inhibiting bacterial TMA production in HC-HFD
199 were decoupled from obesity.
200
201 **TMA treatment mimics choline supplementation.**
202 To further confirm whether TMA mediates the beneficial effects of choline
203 supplementation, we chronically treated LC-HFD-fed C57BL/6 mice with TMA for 6 weeks
204 using subcutaneous osmotic minipumps and assessed their immunometabolism. We
205 confirmed that chronic TMA treatment at 0.01 mM in a LC-HFD did not affect BW gain
206 (**Extended Data Fig. 4g**) but effectively normalised glucose homeostasis and the Matsuda
207 index, a readout of insulin sensitivity (**Fig. 3f-h, Extended Data Fig. 4h**). TMA treatment also
208 improved the pro-inflammatory response to HFD-feeding and hepatic expression of acute
209 phase proteins *Saa1*, *Saa2* and *Saa3* (**Fig. 3i-l**). These results suggest that chronic TMA
210 treatment decouples BW gain and adiposity from low-grade inflammation and glucose
211 homeostasis, thereby mimicking the immune and metabolic benefits observed in choline
212 supplementation.
213
214 **TMA is a IRAK4 kinase inhibitor.**
215 To identify a direct mechanism linking TMA to metabolic and immune benefits in HFD-fed
216 mice, we sought to identify its host pharmacological targets. The kinome, made of 518
217 kinases encoded the human genome[12], represents a repertoire of critical signal transduction
218 switches for metabolic homeostasis and inflammation. To discover specific physical
219 interactions, we screened TMA against a panel of 456 clinically-relevant human kinases
220 using a high-throughput assay[35,36] (see *Methods*) and identified five preliminary hits for TMA
221 (**Fig. 4a** and **Supplementary Table 5**). We then generated multiple-dose binding curves
222 between TMA and each hit and confirmed that TMA physically binds IRAK4 (dissociation
223 constant K_d = 14 nM, **Extended Data Fig. 5a**) but not the other four preliminary hits (flat
224 dissociation curves with no K_d fit in **Extended Data Fig. 5b-e**, suggesting no physical binding
225 was observed). Since K_d only addresses a physical interaction in its simplest form (*i.e.:*
226 binding), we functionally tested TMA as an IRAK4 inhibitor, by quantifying IRAK4 kinase
227 activity in presence of ATP and increasing doses of TMA (see *Methods*) to derive a half-
228 maximal relative inhibitory constant (IC_{50} = 3.4 µM, **Fig. 4b**). We also confirmed that neither
229 choline, TMAO nor DMB inhibit IRAK4 kinase activity (**Extended Data Fig. 5f-h**). We finally

230 confirmed that TMA does not inhibit IRAK-1 either (**Extended Data Fig. 5i**), as suggested by
231 the phenotypic convergence of *Irak-1*$^{-/-}$ mice fed a HFD which were shown to have
232 metabolic improvements similar to TMA treatment[37]. Altogether, this screen shows that
233 IRAK4 is the specific kinase target for TMA, which we next validated using a range of *in vitro*
234 and *in vivo* experiments.
235
236 **TMA inhibits IRAK4 signalling in human PBMCs and primary human hepatocytes.**
237 IRAK4 is a central kinase in the TLR pathway sensing bacterial invasion and promoting a
238 pyretic pro-inflammatory response in infectious contexts[38,39]. To further corroborate the
239 inhibitory action of TMA on IRAK4 on innate immunity, we studied its effect on human
240 peripheral blood mononuclear cells (PBMC) cytokine secretion and NF-κB signalling in
241 response to LPS stimulation, a process exclusively mediated by IRAK4 downstream of TLR4
242 as originally demonstrated by Suzuki et al.[38]. Consistent with this, pre-treatment with TMA
243 for 30 min dose-dependently blunted IL6 and TNFα secretion by PBMCs challenged with LPS
244 after 4 hours (**Fig. 4c, d**). Moreover, IL6 and TNFα secretion was virtually abolished by pre-
245 treatment by the IRAK4 specific inhibitor PF06650833[40] as an additional control (100 nM).
246 Conversely, TMA (100 µM) or the IRAK4 specific inhibitor PF06650833 (100 nM) had no
247 significant impact on TNFα secretion by PBMCs stimulated by phorbol-ester/Ionomycin (**Fig.**
248 **4e**), similarly to human B-cells harbouring IRAK4-inactivating mutations[41]. Taken together,
249 these findings further support our assertion that TMA acts through IRAK4 and further
250 validate the functional inhibition of IRAK4 by TMA in innate immune cells. In addition, TMA
251 (0.1 mM) significantly ameliorated IRAK1 phosphorylation at a site (Thr209) phosphorylated
252 by IRAK4[42] upon short-term stimulation of PBMCs with LPS (up to 60min, **Fig. 4f**). TMA also
253 inhibited ^{Thr209}IRAK1 phosphorylation dose-dependently after LPS stimulation of PBMCs (**Fig.**
254 **4g**). Similarly, TMA time- and dose-dependently suppressed NF-κBp65 phosphorylation in
255 LPS-challenged PBMCs (**Fig. 4h, i**). In agreement with the cellular PBMC experiments a single
256 TMA dose significantly improved mouse survival in a 24-hour LPS septic shock experiment
257 (**Fig. 4j**), which shows similar protection to the Irak4 kinasedead mice[43].
258
259 We then sought to test IRAK4 inhibition in a HFD context, the main free fatty acid (FFA) in
260 our HFD being palmitate, a saturated FFA triggering TLR4 signalling. We therefore used a
261 primary human hepatocyte model of low-grade inflammation and insulin resistance[44].

262 In basal conditions (0 min), TMA (0.1 mM, 30 min) pre-treatment resulted in a significant
263 decrease in $^{pThr345/Ser346}$IRAK4/IRAK4, ^{pThr209}IRAK1/IRAK1 and $^{pSer176/180}$IKKαβ/IKKβ. PA (200
264 µM, 60 min) administration resulted in increased ^{pThr209}IRAK1/IRAK1, $^{pSer176/180}$IKKαβ/IKKβ
265 and ^{pSer536}NF-κBp65/NF-κBp65 (**Extended Data Fig. 6a-d**), which were normalized by TMA
266 treatment. The TMA effect was significant in a 2-way ANOVA for $^{pThr345/Ser346}$IRAK4/IRAK4
267 (p=0.04), ^{pThr209}IRAK1/IRAK1 (p=0.03) and $^{pSer176/180}$IKKαβ/IKKβ (p<0.001). The normalization
268 of the phosphorylation ratios in the TLR4 pathway by TMA resulted in a normalization of PA-
269 induced IL-6 secretion in the cell medium after 4 hours (**Extended Data Fig. 6e**). TMA also
270 prevented the negative impact of PA (200 µM, 4 h) on insulin action (specifically on insulin-
271 induced ^{pSer473}Akt1/Akt1), indicating a beneficial TMA effect on insulin signaling (**Extended**
272 **Data Fig. 6f**). TMA also tended to decrease $^{pThr183/Tyr185}$SAPK/JNK/SAPK/JNK induced by PA
273 (200 µM, 60 min, **Extended Data Fig. 5j**) but had no significant effect on p38MAPK
274 (**Extended Data Fig. 5k**). Collectively, our results demonstrate that TMA is an IRAK4 kinase
275 inhibitor ameliorating LPS inflammatory signalling in PBMCs and mice and normalising
276 palmitate-induced low-grade inflammation and aberrant insulin signalling *in vitro*, requiring
277 further assessment in *Irak4*$^{-/-}$ mice.
278
279 ***Irak4*$^{-/-}$ mice are protected against HFD-induced immune and metabolic dysregulations.**
280 IRAK4 is a key kinase required for defence against pyogenic infections in acute contexts[38,39].
281 To further test whether this kinase plays a role in HFD-induced chronic low-grade
282 inflammation and glucose homeostasis, we fed 5-week-old *Irak4*$^{-/-}$ mice[45] and wild-type
283 (WT) littermates in C57BL/6 background (**Extended Data Fig. 7a** for genotyping) a LC-HFD, to
284 avoid potential confounding effects from TMA for 8 weeks before assessing circulating
285 cytokines, expression of hepatic inflammatory genes and acute-phase markers and
286 metabolic homeostasis (**Fig. 5a-h**). Irak4$^{-/-}$ mice presented improved glycemic control
287 compared to wild-type littermates (**Fig.5 a,b**). Likewise, the inflammatory response to LC-
288 HFD observed in WT was obliterated in *Irak4*$^{-/-}$ littermates (**Fig. 5c-g**). There was a similar
289 trend for *Saa3* (**Fig. 5h**), whilst there was no effect on BW gains (**Extended Data Fig. 7b**).
290 Hence, similarly to TMA treatment, genetic ablation of IRAK4 abolishes the HFD-induced
291 pro-inflammatory response and IGT thereby decoupling obesity from impaired glucose
292 tolerance and low-grade inflammation with a similar phenotype to *Irak1* deficiency[37].
293

294 **Pharmacological inhibition of Irak4 normalises glucose metabolism.**

295 Since the *Irak4*$^{-/-}$ mice lack the whole protein, we compared the knock-out phenotype with
296 the phenotype of PF06650833, a recently discovered chemical inhibitor of the human IRAK4
297 protein[40] with promising results in a phase-I trial for rheumatoid arthritis[46]. Treatment with
298 PF06650833 improved BW in LC-HFD mice (**Extended Data Fig. 7c**). This inhibitor also
299 yielded significant improvements in plasma glycemia at the latter time-points of the GTT
300 and insulin tolerance test (ITT) and in cumulative glycemia (**Fig. 5i-l**), which was mirrored by
301 an increase in Akt phosphorylation (**Fig. 5m-n**). These results collectively show that specific
302 chemical inhibition of IRAK4 leads to significant improvements in glycemic control, insulin
303 sensitivity and insulin signalling. Further, they suggest that IRAK4 could constitute a clinically
304 relevant target in IR and related disorders.

305

306 **DISCUSSION**

307 The discovery that TMA is a kinase inhibitor controlling IRAK4, a central kinase involved in
308 innate immunity, is a major finding that provides an attractive mechanism for the metabolic
309 and immune improvements observed with choline-supplementation in HFD contexts (**Fig.**
310 **6**).

311

312 IRAK4 is the first regulatory checkpoint downstream of MyD88, the adapter protein
313 connecting IRAK4 to at least six TLRs sensing bacterial compounds/components[47]. IRAK4
314 deficiency is associated with bacterial infections in humans[39] and in mice[48]. Consistent with
315 the involvement of the TLR signalling pathway at the crossroads between gut microbiota
316 and dietary lipids[49,50], IRAK4 deletion and its inhibition by TMA and PF06650833[40] rescued
317 HFD-induced low-grade inflammation and IR[3,51,52], highlighting new and unexpected roles
318 for this microbial metabolite and its target kinase in immunometabolism. The relative IC_{50}
319 (3.4 µM) we determined is two times smaller than the plasma isotopic quantifications
320 obtained by UPLC-MS/MS in the HFD group supplemented with choline. These
321 quantifications are comparable to circulating TMA levels previously reported in normal
322 human plasma, ranging between 0.42 and 48 µM[53,54], which makes this IC_{50} particularly
323 relevant with respect to pathophysiological mechanisms: dosing mice with 0.01 mM TMA
324 (3x IC_{50}) was sufficient to improve inflammatory and metabolic responses. TMA can
325 therefore be considered a "microbial signalling metabolite"[55] sending a negative feedback

326 signal to a pathway triggered by influx of saturated free fatty acids in HFD contexts, this
327 mechanism participating in maintaining a low immunological footprint and improved
328 metabolic homeostasis in a symbiotic relationship. TMA's role as an IRAK4 inhibitor could,
329 for instance, explain some of the beneficial effects reported for choline supplementation in
330 NAFLD patients[56] and of improved IR observed in those consuming higher choline diets in a
331 healthy genetically uniform human population[57]. Altogether, our results on IRAK4 inhibition
332 and ablation provide further insight in the phenotypic convergence between *Myd88*, *Irak4*
333 and *Irak1* knock-out mouse models[37,58], suggesting that the gut microbiota, through TMA,
334 proceeds with a targeted "hijacking" of the TLR signal transduction machinery to the host's
335 benefit resulting in metabolic and immune improvements.
336
337 Our finding that TMA improves metabolic health in the context of HFD is surprising given
338 the extensive evidence linking higher levels of circulating TMAO (after phase-1 *N*-oxidation
339 of TMA in the liver) with worst cardiovascular outcomes, particularly in patients with
340 established atherosclerosis and thrombosis[14]. Our results show that the TMA-lyase inhibitor
341 DMB blocks TMA production and abrogates the metabolic benefits brought by choline
342 supplementation in the HC-HFD mice, suggesting that the benefits come from conversion of
343 choline to TMA. Our findings are supported by the discovery that in diabetic mice
344 knockdown of the liver gene (*fmo3*) that converts TMA to TMAO, an intervention that would
345 increase TMA levels, improves IR and attenuates atherosclerotic burden[23]. Similarly, in an
346 epidemiological study in a genetically homogeneous population, higher choline
347 consumption associated with improved insulin sensitivity[57].
348
349 Our work is consistent with the idea that TMA and TMAO may well play contrasting roles
350 that are mechanism- and context-dependent. To illustrate context dependence, TMAO,
351 which has been associated with poor cardiovascular outcomes in humans also beneficially
352 reduces blood-brain barrier permeability[59], independently of its role in CVD. To illustrate the
353 target-dependence, TMAO augments Ca^{2+}-mediated platelet aggregation after thrombin
354 treatment. TMAO also binds to and activates purified Protein Kinase RNA-Like ER Kinase
355 (PERK) whilst structurally related metabolites such as choline do not[60]. Similarly, we
356 discovered that TMA binds to and inhibits IRAK4 whilst TMAO does not (ED figure 5g),
357 suggesting an unexpected and independent mechanism of action. Our observations on

358 IRAK4 inhibition by TMA and in *Irak4* knock-out mice are consistent with observations in
359 Myd88 and Irak1 knock-out mice, resulting in improved glucose tolerance and insulin
360 sensitivity. Consistent with our observations, *Fmo3* deletion, which as a result prevents *N*-
361 oxidation of TMA into TMAO, improved IR in mice[23]. Therefore, we submit that our study
362 reveals divergent context-dependent actions between TMA and its phase-II metabolite
363 TMAO in an HFD context in a "yin-yang relationship".
364
365 In conclusion, through the combination of *ex vivo*, *in vitro* and *in vivo* approaches, we reveal
366 a unique mechanism in which TMA acts as a gut microbial signalling metabolite inhibiting
367 IRAK4, a central molecular target in the TLR pathway, thereby allowing the gut microbiota to
368 control HFD-induced pro-inflammatory response(s) and IR. The kinome represents a key
369 repertoire of regulatory host targets for microbial signals and the uncharted microbiome–
370 kinome crosstalk requires further investigation. Our work can guide human trials where the
371 efficacy of IRAK4 inhibitors available for human use or dietary interventions that increase
372 TMA bioavailability can be evaluated in the context of obesity and IR. Moreover, since IR is
373 an independent risk factor of CVD in humans[61], our work uncovers a novel strategy to
374 alleviate obesity-associated increased cardiovascular risk. By highlighting the physiological
375 and therapeutic roles of TMA and IRAK4 on HFD-induced low-grade inflammation and IR, we
376 anticipate that its immunomodulatory properties extend beyond IR to a wider range of
377 human pathologies involving TLR signalling and modulation of innate immunity.
378
379
380 **Author Contributions.**
381 JC, PA, BAS and SG performed cell-based assays, JC performed multivariate statistics and
382 interpreted the results. JC, FB, JFF, AE, HP, LZ, DS, ARR, PDC, VC, RM, SC and CG contributed
383 *in vivo* experiments, RHB, AM, ALN, LMG, SG, JMMN, JL, CLB and SP performed various
384 experiments. LH analysed microarray data. JS, DG, JKN, PPL, PDC, JMFR, NJG and MED
385 conceived the project, mentored and supervised its participants and interpreted its results.
386 MED performed metabolic profiling experiments, analysed data and interpreted the results.
387 JC, PA, NJG, DG, PPL, PDC, and MED wrote the manuscript. All authors edited and approved
388 the manuscript.
389

Acknowledgments.

This work was supported by grants from the Wellcome Trust (Functional Genomics Initiative grant Biological Atlas of Insulin Resistance 06678 to JKN, DG and JS) and the European Commission (METACARDIS HEALTH-F4-2012-305312 to DG and MED, Institut Mérieux through a grant awarded to MED, Spanish Institute of Health Research (FIS) grant (PI18/01022 and PI21/01361), by Fondo Europeo de Desarrollo Regional (FEDER) funds, the Catalan Government (AGAUR, #SGR2017-00734, ICREA Academia Award 2021) to JMFR and Canadian Institutes of Health Research (CIHR) grants (MOP-49413 & MOP-142471) awarded to PPL. The laboratory of M.E.D. has received funding by the UK Medical Research Council (MRC grants "µNeuroInf" MR/M501797/1 and "National Mouse Genetics Network Microbiome Cluster" MR/W022532/1), and by grants from the French National Research Agency (ANR-10-LABX-46 [European Genomics Institute for Diabetes]), from the National Center for Precision Diabetic Medicine – PreciDIAB, which is jointly supported by the French National Agency for Research (ANR-18-IBHU-0001), by the European Union (FEDER), by the Hauts-de-France Regional Council (Agreement 20001891/NP0025517) and by the European Metropolis of Lille (MEL, Agreement 2019_ESR_11) and by Isite ULNE (R-002-20-TALENT-DUMAS), also jointly funded by ANR (ANR-16-IDEX-0004-ULNE), the Hauts-de-France Regional Council (20002845) and by the European Metropolis of Lille (MEL). This research was also supported by the National Institute for Health Research (NIHR) Imperial Biomedical Research Centre (MED, S.D.G.). DG held a Wellcome Trust Senior Fellowship in Basic Biomedical Science (057733). JEF was supported by the Medical Research Council (grant number MR/K020919/1). PA is the recipient of a Career Development Award from the Medical Research Council (Grant No. MR/Y010051/1). PDC is a senior research associate and AE a research associate at FRS-FNRS (Fonds de la Recherche Scientifique). PDC is the recipient of grants from FNRS. LH was in receipt of an MRC Intermediate Research Fellowship in Data Science (grant number MR/L01632X/1, UK Med-Bio). This work was supported by FRFS-WELBIO under grant: WELBIO-CGR-2017, by the Funds InBev-Baillet Latour (Grant for Medical Research 2015) and ERC Starting Grant 2013 (European Research Council, Starting grant 336452-ENIGMO).

Online Content.

Methods, along with any additional Supplementary display items and Source Data, are available in the online version of the paper; references unique to these sections appear only in the online paper.

426 **References.**

427 1. Ong, K. L. *et al.* Global, regional, and national burden of diabetes from 1990 to 2021,
428 with projections of prevalence to 2050: a systematic analysis for the Global Burden of
429 Disease Study 2021. *The Lancet* **402**, 203–234 (2023).
430 2. Samuel, V. T. & Shulman, G. I. Mechanisms for Insulin Resistance: Common Threads
431 and Missing Links. *Cell* **148**, 852–871 (2012).
432 3. Cai, D. *et al.* Local and systemic insulin resistance resulting from hepatic activation of
433 IKK-β and NF-κB. *Nat. Med.* **11**, 183–190 (2005).
434 4. Wu, G. D. *et al.* Linking Long-Term Dietary Patterns with Gut Microbial Enterotypes.
435 *Science* **334**, 105–108 (2011).
436 5. Le Chatelier, E. *et al.* Richness of human gut microbiome correlates with metabolic
437 markers. *Nature* **500**, 541–546 (2013).
438 6. Pedersen, H. K. *et al.* Human gut microbes impact host serum metabolome and
439 insulin sensitivity. *Nature* **535**, 376–381 (2016).
440 7. Cani, P. D. *et al.* Metabolic Endotoxemia Initiates Obesity and Insulin Resistance.
441 *Diabetes* **56**, 1761–1772 (2007).
442 8. Hooper, L. V., Littman, D. R. & Macpherson, A. J. Interactions Between the
443 Microbiota and the Immune System. *Science* **336**, 1268–1273 (2012).
444 9. Nicholson, J. K. *et al.* Host-Gut Microbiota Metabolic Interactions. *Science* **336**, 1262–
445 1267 (2012).
446 10. Maslowski, K. M. *et al.* Regulation of inflammatory responses by gut microbiota and
447 chemoattractant receptor GPR43. *Nature* **461**, 1282–1286 (2009).
448 11. Venkatesh, M. *et al.* Symbiotic Bacterial Metabolites Regulate Gastrointestinal
449 Barrier Function via the Xenobiotic Sensor PXR and Toll-like Receptor 4. *Immunity* **41**, 296–
450 310 (2014).
451 12. Manning, G., Whyte, D. B., Martinez, R., Hunter, T. & Sudarsanam, S. The Protein
452 Kinase Complement of the Human Genome. *Science* **298**, 1912–1934 (2002).
453 13. Dumas, M.-E. *et al.* Metabolic profiling reveals a contribution of gut microbiota to
454 fatty liver phenotype in insulin-resistant mice. *Proc. Natl. Acad. Sci.* **103**, 12511–12516
455 (2006).
456 14. Wang, Z. *et al.* Gut flora metabolism of phosphatidylcholine promotes cardiovascular
457 disease. *Nature* **472**, 57–63 (2011).
458 15. Al-Waiz, M., Mikov, M., Mitchell, S. C. & Smith, R. L. The exogenous origin of
459 trimethylamine in the mouse. *Metabolism* **41**, 135–136 (1992).
460 16. Craciun, S. & Balskus, E. P. Microbial conversion of choline to trimethylamine
461 requires a glycyl radical enzyme. *Proc. Natl. Acad. Sci.* **109**, 21307–21312 (2012).
462 17. Koeth, R. A. *et al.* Intestinal microbiota metabolism of l-carnitine, a nutrient in red
463 meat, promotes atherosclerosis. *Nat. Med.* **19**, 576–585 (2013).
464 18. Al-Waiz, M., Ayesh, R., Mitchell, S. C., Idle, J. R. & Smith, R. L. Disclosure of the
465 metabolic retroversion of trimethylamine N-oxide in humans: A pharmacogenetic approach.
466 *Clin. Pharmacol. Ther.* **42**, 608–612 (1987).
467 19. Hoyles, L. *et al.* Metabolic retroconversion of trimethylamine N-oxide and the gut
468 microbiota. *Microbiome* **6**, 73 (2018).
469 20. Dolphin, C. T., Janmohamed, A., Smith, R. L., Shephard, E. A. & Phillips, Ian R.
470 Missense mutation in flavin-containing mono-oxygenase 3 gene, FMO3, underlies fish-odour
471 syndrome. *Nat. Genet.* **17**, 491–494 (1997).

472 21. Shih, D. M. *et al.* Flavin containing monooxygenase 3 exerts broad effects on glucose
473 and lipid metabolism and atherosclerosis. *J. Lipid Res.* **56**, 22–37 (2015).
474 22. Warrier, M. *et al.* The TMAO-Generating Enzyme Flavin Monooxygenase 3 Is a
475 Central Regulator of Cholesterol Balance. *Cell Rep.* **10**, 326–338 (2015).
476 23. Morbid Obesity Study Group *et al.* Flavin-containing monooxygenase 3 as a potential
477 player in diabetes-associated atherosclerosis. *Nat. Commun.* **6**, 6498 (2015).
478 24. Schugar, R. C. *et al.* The TMAO-Producing Enzyme Flavin-Containing Monooxygenase
479 3 Regulates Obesity and the Beiging of White Adipose Tissue. *Cell Rep.* **19**, 2451–2461
480 (2017).
481 25. Özcan, U. *et al.* Endoplasmic Reticulum Stress Links Obesity, Insulin Action, and Type
482 2 Diabetes. *Science* **306**, 457–461 (2004).
483 26. Eckel-Mahan, K. L. *et al.* Reprogramming of the Circadian Clock by Nutritional
484 Challenge. *Cell* **155**, 1464–1478 (2013).
485 27. Thorens, B. *et al.* Use of preclinical models to identify markers of type 2 diabetes
486 susceptibility and novel regulators of insulin secretion – A step towards precision medicine.
487 *Mol. Metab.* **27**, S147–S154 (2019).
488 28. Dumas, M.-E. *et al.* Microbial-Host Co-metabolites Are Prodromal Markers Predicting
489 Phenotypic Heterogeneity in Behavior, Obesity, and Impaired Glucose Tolerance. *Cell Rep.*
490 **20**, 136–148 (2017).
491 29. Fromentin, S. *et al.* Microbiome and metabolome features of the cardiometabolic
492 disease spectrum. *Nat. Med.* **28**, 303–314 (2022).
493 30. Forslund, S. K. *et al.* Combinatorial, additive and dose-dependent drug–microbiome
494 associations. *Nature* **600**, 500–505 (2021).
495 31. Matsuda, M. & DeFronzo, R. A. Insulin sensitivity indices obtained from oral glucose
496 tolerance testing: comparison with the euglycemic insulin clamp. *Diabetes Care* **22**, 1462–
497 1470 (1999).
498 32. Liu, H.-Y. *et al.* Increased basal level of Akt-dependent insulin signaling may be
499 responsible for the development of insulin resistance. *Am. J. Physiol. Endocrinol. Metab.*
500 **297**, E898-906 (2009).
501 33. Sack, G. H. Serum amyloid A – a review. *Mol. Med.* **24**, 46 (2018).
502 34. Wang, Z. *et al.* Non-lethal Inhibition of Gut Microbial Trimethylamine Production for
503 the Treatment of Atherosclerosis. *Cell* **163**, 1585–1595 (2015).
504 35. Fabian, M. A. *et al.* A small molecule–kinase interaction map for clinical kinase
505 inhibitors. *Nat. Biotechnol.* **23**, 329–336 (2005).
506 36. Karaman, M. W. *et al.* A quantitative analysis of kinase inhibitor selectivity. *Nat.*
507 *Biotechnol.* **26**, 127–132 (2008).
508 37. Sun, X.-J. *et al.* Deletion of interleukin 1 receptor-associated kinase 1 (Irak1)
509 improves glucose tolerance primarily by increasing insulin sensitivity in skeletal muscle. *J.*
510 *Biol. Chem.* **292**, 12339–12350 (2017).
511 38. Suzuki, N. *et al.* Severe impairment of interleukin-1 and Toll-like receptor signalling in
512 mice lacking IRAK-4. *Nature* **416**, 750–754 (2002).
513 39. Picard, C. *et al.* Pyogenic Bacterial Infections in Humans with IRAK-4 Deficiency.
514 *Science* **299**, 2076–2079 (2003).
515 40. Lee, K. L. *et al.* Discovery of Clinical Candidate 1-{[(2 *S* ,3 *S* ,4 *S*)-3-Ethyl-4-fluoro-5-
516 oxopyrrolidin-2-yl]methoxy}-7-methoxyisoquinoline-6-carboxamide (PF-06650833), a
517 Potent, Selective Inhibitor of Interleukin-1 Receptor Associated Kinase 4 (IRAK4), by
518 Fragment-Based Drug Design. *J. Med. Chem.* **60**, 5521–5542 (2017).

519 41. Ku, C.-L. *et al.* Selective predisposition to bacterial infections in IRAK-4–deficient
520 children: IRAK-4–dependent TLRs are otherwise redundant in protective immunity. *J. Exp.*
521 *Med.* **204**, 2407–2422 (2007).
522 42. Kollewe, C. *et al.* Sequential Autophosphorylation Steps in the Interleukin-1
523 Receptor-associated Kinase-1 Regulate its Availability as an Adapter in Interleukin-1
524 Signaling. *J. Biol. Chem.* **279**, 5227–5236 (2004).
525 43. Kim, T. W. *et al.* A critical role for IRAK4 kinase activity in Toll-like receptor–mediated
526 innate immunity. *J. Exp. Med.* **204**, 1025–1036 (2007).
527 44. Hoyles, L. *et al.* Molecular phenomics and metagenomics of hepatic steatosis in non-
528 diabetic obese women. *Nat. Med.* **24**, 1070–1080 (2018).
529 45. Valaperti, A. *et al.* Innate Immune Interleukin-1 Receptor–Associated Kinase 4
530 Exacerbates Viral Myocarditis by Reducing CCR5 $^{+}$ CD11b $^{+}$ Monocyte Migration and
531 Impairing Interferon Production. *Circulation* **128**, 1542–1554 (2013).
532 46. Winkler, A. *et al.* The Interleukin-1 Receptor–Associated Kinase 4 Inhibitor PF-
533 06650833 Blocks Inflammation in Preclinical Models of Rheumatic Disease and in Humans
534 Enrolled in a Randomized Clinical Trial. *Arthritis Rheumatol.* **73**, 2206–2218 (2021).
535 47. O'Neill, L. A. J., Golenbock, D. & Bowie, A. G. The history of Toll-like receptors —
536 redefining innate immunity. *Nat. Rev. Immunol.* **13**, 453–460 (2013).
537 48. von Bernuth, H., Picard, C., Puel, A. & Casanova, J.-L. Experimental and natural
538 infections in MyD88- and IRAK-4-deficient mice and humans: HIGHLIGHTS. *Eur. J. Immunol.*
539 **42**, 3126–3135 (2012).
540 49. Caesar, R., Tremaroli, V., Kovatcheva-Datchary, P., Cani, P. D. & Bäckhed, F. Crosstalk
541 between Gut Microbiota and Dietary Lipids Aggravates WAT Inflammation through TLR
542 Signaling. *Cell Metab.* **22**, 658–668 (2015).
543 50. Shi, H. *et al.* TLR4 links innate immunity and fatty acid–induced insulin resistance. *J.*
544 *Clin. Invest.* **116**, 3015–3025 (2006).
545 51. Reilly, S. M. *et al.* An inhibitor of the protein kinases TBK1 and IKK-ε improves
546 obesity-related metabolic dysfunctions in mice. *Nat. Med.* **19**, 313–321 (2013).
547 52. Kiechl, S. *et al.* Blockade of receptor activator of nuclear factor-κB (RANKL) signaling
548 improves hepatic insulin resistance and prevents development of diabetes mellitus. *Nat.*
549 *Med.* **19**, 358–363 (2013).
550 53. Bain, M. A., Faull, R., Fornasini, G., Milne, R. W. & Evans, A. M. Accumulation of
551 trimethylamine and trimethylamine-N-oxide in end-stage renal disease patients undergoing
552 haemodialysis. *Nephrol. Dial. Transplant.* **21**, 1300–1304 (2006).
553 54. Lundh, T., Akesson, B. & Skerfving, S. Effect of dietary intake of trimethylamine on
554 human metabolism of the industrial catalyst dimethylethylamine. *Occup. Environ. Med.* **52**,
555 478–483 (1995).
556 55. Dumas, M.-E. The Microbial-Mammalian Metabolic Axis: Beyond Simple Metabolism.
557 *Cell Metab.* **13**, 489–490 (2011).
558 56. Spencer, M. D. *et al.* Association Between Composition of the Human
559 Gastrointestinal Microbiome and Development of Fatty Liver With Choline Deficiency.
560 *Gastroenterology* **140**, 976–986 (2011).
561 57. Gao, X., Wang, Y. & Sun, G. High dietary choline and betaine intake is associated with
562 low insulin resistance in the Newfoundland population. *Nutrition* **33**, 28–34 (2017).
563 58. Everard, A. *et al.* Intestinal epithelial MyD88 is a sensor switching host metabolism
564 towards obesity according to nutritional status. *Nat. Commun.* **5**, 5648 (2014).

565 59. Hoyles, L. *et al.* Regulation of blood–brain barrier integrity by microbiome-associated
566 methylamines and cognition by trimethylamine N-oxide. *Microbiome* **9**, 235 (2021).
567 60. Chen, S. *et al.* Trimethylamine N-Oxide Binds and Activates PERK to Promote
568 Metabolic Dysfunction. *Cell Metab.* **30**, 1141-1151.e5 (2019).
569 61. Laakso, M. & Kuusisto, J. Insulin resistance and hyperglycaemia in cardiovascular
570 disease development. *Nat. Rev. Endocrinol.* **10**, 293–302 (2014).
571 62. Ahmetaj-Shala, B. *et al.* A bioassay system of autologous human endothelial, smooth
572 muscle cells, and leukocytes for use in drug discovery, phenotyping, and tissue engineering.
573 *FASEB J.* **34**, 1745–1754 (2020).
574 63. Latorre, J. *et al.* Decreased lipid metabolism but increased FA biosynthesis are
575 coupled with changes in liver microRNAs in obese subjects with NAFLD. *Int. J. Obes.* **41**, 620–
576 630 (2017).
577 64. Toye, A. A. *et al.* Subtle metabolic and liver gene transcriptional changes underlie
578 diet-induced fatty liver susceptibility in insulin-resistant mice. *Diabetologia* **50**, 1867–1879
579 (2007).
580 65. Geurts, L., Muccioli, G. G., Delzenne, N. M. & Cani, P. D. Chronic Endocannabinoid
581 System Stimulation Induces Muscle Macrophage and Lipid Accumulation in Type 2 Diabetic
582 Mice Independently of Metabolic Endotoxaemia. *PLoS ONE* **8**, e55963 (2013).
583 66. *Bioinformatics and Computational Biology Solutions Using R and Bioconductor*.
584 (Springer New York, New York, NY, 2005). doi:10.1007/0-387-29362-0.
585 67. Smyth, G. K. limma: Linear Models for Microarray Data. in *Bioinformatics and*
586 *Computational Biology Solutions Using R and Bioconductor* (eds. Gentleman, R., Carey, V. J.,
587 Huber, W., Irizarry, R. A. & Dudoit, S.) 397–420 (Springer-Verlag, New York, 2005).
588 doi:10.1007/0-387-29362-0_23.
589 68. Chen, E. Y. *et al.* Enrichr: interactive and collaborative HTML5 gene list enrichment
590 analysis tool. *BMC Bioinformatics* **14**, 128 (2013).
591 69. Tarca, A. L. *et al.* A novel signaling pathway impact analysis. *Bioinformatics* **25**, 75–82
592 (2009).
593 70. Lee, J.-M. *et al.* Serum amyloid A3 exacerbates cancer by enhancing the suppressive
594 capacity of myeloid-derived suppressor cells via TLR2-dependent STAT3 activation: Cellular
595 immune response. *Eur. J. Immunol.* **44**, 1672–1684 (2014).
596 71. Plovier, H. *et al.* A purified membrane protein from Akkermansia muciniphila or the
597 pasteurized bacterium improves metabolism in obese and diabetic mice. *Nat. Med.* **23**, 107–
598 113 (2017).
599 72. Blaise, B. J. *et al.* Metabotyping of *Caenorhabditis elegans* reveals latent phenotypes.
600 *Proc. Natl. Acad. Sci.* **104**, 19808–19812 (2007).
601
602

603 **Online Methods**

604 **Protocols**

605 All experimental procedures involving mice were carried out in accordance with U.K. Home
606 Office, Canadian Council on Animal Care, the ethics committee of the French Research
607 Ministry (authorization number 00486.01), Belgian Law of May 29, 2013 regarding the
608 protection of laboratory animals (agreement number LA1230314) and local guidelines on
609 animal welfare and license conditions and the University of Oxford, University of Ottawa,
610 Université Pierre et Marie Curie and Université catholique de Louvain guidelines on animal
611 welfare.

612

613 **PBMC isolation and cell-based assays**

614 PBMCs were isolated as previously described[62] following local ethical approval from Imperial
615 College Research Ethics Committee (19IC5372). Briefly, human peripheral blood samples (32
616 ml) were collected from donors in BD Vacutainer Cell Preparation Tubes containing Sodium
617 Heparin/Ficoll (BD Biosciences, UK). PBMCs were separated by centrifugation at 1600 ***g*** for
618 30 min at room temperature, followed by three washing steps with PBS and 10% FBS
619 (LabTech, UK), and were centrifuged at 520 RCF for 10 min after each wash. Donors were
620 females aged between 25 and 32 years. All subjects were healthy volunteers by self-
621 declaration and provided written informed consent.

622

623 **LPS stimulation and IL6 and TNFα release quantification**.

624 Human PBMCs ($1x10^5$ per condition in duplicate), freshly isolated as described above, were
625 serum-starved in 0.1% v/v FCS RPMI-1640 (Sigma Cat. R7638) in the presence of TMA (Sigma
626 Cat.No. 72761) or the IRAK4 inhibitor PF06650833 (0.5µM; Tocris Cat.No.6373; PF
627 thereafter), as indicated in the corresponding Figures, for 30 min. PBMCs were subsequently
628 stimulated with 1 µg/ml LPS (Sigma Cat.No. L2630) for 4 h (37 ^oC, 5% CO_2). For the
629 PMA/Ionomycin stimulation experiments, human PBMCs isolated as above ($1x10^5$ per
630 condition) pre-incubated with TMAO (100 µM), PF06650833 (0.5µM) or vehicle as indicated
631 for 30min were then stimulated with 50ng/ml Phorbol 12-myristate 13-acetate (PMA; Sigma
632 Cat.No. 79346) and 1µg/ml ionomycin (Sigma Cat.No. I0634) for 4h. Next cells were pelleted
633 by centrifugation (200 ***g*** for 10 min) and supernatants were collected and stored at -20 ^oC

634 until further use. IL6 and TNFα were measured in the media diluted 1:10 in RPMI-1640 using
635 the DuoSet ELISA kits from R&D (Cat.No. DY206 and Cat.No. DY210 from R&D, respectively)
636 according to the manufacturer's instructions. For PMA/ionomycin TNFα measurements the
637 media were un-diluted. For all treatments *N*=4 biological repeats.
638
639 **PBMCs IRAK1 and NF-κBp65 phosphorylation in response to LPS.**

640 Freshly isolated human PBMCs ($1x10^6$/ml per condition) were added to 96-well plates
641 coated with *L*-poly-lysine for 30 min (100 ng/ml, Sigma Cat.No. P4707) in RPMI-1640
642 containing 20% FCS and were left to attach to the wells overnight at 37 ^oC, 5% CO_2. The
643 following day media were discarded and cells were incubated in serum-free RPMI-1640
644 containing 100 µM TMA, or RPMI-1640 vehicle for 30 min. PBMCs were then stimulated
645 with LPS (1 µg/ml) for the indicated times in corresponding Figure legends, for up to 60 min.
646 At the end of the stimulation PBMCs were fixed with 8% paraformaldehyde (Sigma Cat.No.
647 F8775) at room temperature for 20 min. Phosphorylation of IRAK1 (at Thr209) or NF-κBp65
648 (at Ser536) was determined in fixed PBMCs using commercially available ELISA kits
649 (Cat.No.LS-F1401-1 or Cat.No.LS-F891-1 respectively, both from LSBio) according to the
650 manufacturer's instructions. Readings were normalized to the levels of total-IRAK1 protein
651 determined in sister wells treated identically. The dose-dependent impact of TMA (see
652 corresponding Figures) on phospho levels of IRAK1 or NF-κBp65 upon LPS (1 µg/ml)
653 stimulation of PBMCs (for 10 min or 15 min, respectively) was also determined using the
654 commercially available kits from LSBio as described above.
655
656 **Cell-based assays in primary human hepatocytes.**
657 Cryopreserved primary human hepatocytes (HH) were commercially sourced (Innoprot,
658 Bizkaia, Spain) and cultured with hepatocytes medium (Innoprot) supplemented with 5%
659 fetal bovine serum, 1% hepatocytes growth supplement (mixture of growth factors,
660 hormones and proteins necessary for culture of primary hepatocytes) and 100 U/mL
661 penicillin and streptomycin. HH were grown on poly-*L*-lysine pre-coated cell dishes at 37 °C
662 and 5% CO_2 atmosphere following manufacturer's recommendations. The following
663 experiments were performed 24 h after seeding: i) First, palmitic acid (PA, 200 µM)
664 administration (0 and 60 min) with or without trimethylamine hydrochloride (TMA, 0.1 mM,

665 30 min) pre-treatment plus co-administration during PA exposure were assayed. PA solution
666 was prepared as previously reported[44,63]. In this experiment, the effect of PA and TMA on
667 IRAK1, IRAK4, NF-κBp65, IKKαβ, SAPK/JNK and p38MAPK activity was analyzed. ii) In a
668 second experiment, the effect of TMA (0.1 mM, 30 min) pre-treatment plus co-
669 administration during vehicle or PA exposure for 4 h on insulin action and on IL6 release
670 were tested. Insulin action was evaluated measuring ^{pSer473}Akt1/Akt1 after insulin (100 nM,
671 10 min) stimuli.
672 ^{pThr209}IRAK1, total IRAK1, ^{pSer536}NF-κBp65, total NF-κBp65, ^{pSer473}AKT1, total AKT1 and GAPDH
673 (as an endogenous control) were measured with specific colorimetric Cell-Based ELISA Kits
674 [CytoGlow™ IRAK1 (catalog nº: CBP1425), CytoGlow™ NF-κBp65 (catalog nº: CBP1633) and
675 CytoGlow™ AKT1 (catalog nº: CBP1490), Assay Biotechnology Company, Inc, CA, USA]
676 following manufacturer's instructions. For data analysis, optical density of target proteins
677 (read at 450 nm) was normalized with cell nuclei crystal violet staining (read at 595 nm),
678 which was proportional to cell counts. The analysis of cell-based assays was performed in a
679 blind manner.
680 $^{pThr345/Ser346}$IRAK4/IRAK4, $^{pSer176/180}$IKKαβ/IKKβ, $^{pThr183/Tyr185}$SAPK/JNK and
681 $^{pThr180/Tyr182}$p38MAPK/p38MAPK were determined by western blot. Briefly, hepatocyte
682 proteins were directly extracted in radioimmnuno precipitation assay (RIPA) buffer (0.1%
683 SDS, 0.5% sodium deoxycholate, 1% Nonidet P-40, 150 mM NaCl, and 50 mM Tris-HCl, pH
684 8.0), supplemented with protease inhibitors (1 mM phenylmethylsulfonyl fluoride). Cellular
685 debris and lipids were eliminated by centrifugation of the solubilized samples at 13000 rpm
686 for 10 min at 4 °C, recovering the soluble fraction. Protein concentration was determined
687 using the RC/DC Protein Assay (Bio-Rad Laboratories, Hercules, CA). RIPA protein extracts
688 (20 µg) were separated by SDS-PAGE and transferred to nitrocellulose membranes by
689 conventional procedures. Membranes were immunoblotted with antibodies against the
690 following proteins: $^{pThr345/Ser346}$IRAK4 (#11927), IRAK4 (#4363), $^{pSer176/180}$IKKαβ (#2694), IKKβ
691 (#8943), $^{pThr183/Tyr185}$SAPK/JNK (4668), SAPK/JNK (#9258), $^{pThr180/Tyr182}$p38MAPK (#9215),
692 p38MAPK (#9212), all purchased from Cell Signaling Technology, Inc (CST, MA, USA) and β-
693 actin (sc-47778, Santa Cruz Biotechnology, CA, USA). Anti-rabbit IgG and anti-mouse IgG
694 coupled to horseradish peroxidase was used as a secondary antibody. Horseradish
695 peroxidase activity was detected by chemiluminescence, and quantification of protein
696 expression was performed using scion image software. IL6 concentration in hepatocyte

697 media was measured using Human IL-6 Quantikine ELISA Kit (D6050, R&D Systems, Inc, MN,
698 USA). All these experiments were performed at least in three sample replicates.
699
700 **Mouse Models.**
701 Longitudinal HFD-feeding in mice. All experiments were approved by the ethical committee
702 of the University of Oxford. Male mice from C57BL/6J inbred strain were bred in our animal
703 facility by using a stock originating from The Jackson Laboratory. At 5 weeks of age, groups
704 of n=8-10 mice were transferred to a 40 % w/w HFD (65% kcal) (Special Diets Services),
705 containing 32 % lard and 8 % corn oil, whereas control groups remained on a 5 % Low Fat
706 Diet (CHD) (B & K Universal) for up to 6 months. Detailed diet formulations were published
707 previously[13] and summarised in **Supplementary Table 6**.
708
709 Mice were housed under a 12 h–12 h light–dark cycle. For physiological profiling, several
710 mouse groups fed CHD or HFD were tested to assess consistency of results and discard any
711 impact of potential batch effects. Intra peritoneal glucose tolerance tests (ipGTTs) were
712 performed in mice after 2-, 3-, 5-and 7-month-old mice after an overnight fast, as previously
713 published[64] (see also metabolic phenotyping below). Four days after the GTT, 24 h urinary
714 samples (9 a.m. to 9 a.m.) were collected from mice maintained in individual metabolic
715 cages. Urinary samples collected in a solution of 1 % (wt/vol) sodium azide were centrifuged
716 to remove solid particles and kept at -80 °C until assayed. After an overnight fast, mice were
717 killed by exsanguination. Plasma was separated by centrifugation and stored at -80 °C until
718 ^{1}H-NMR analysis.
719
720 *Choline supplementation on HFD.* At 5 weeks of age, mice were fed either a chow diet
721 containing 2 g of choline/kg of diet (Research Diets, D12450J), a low-choline HFD containing
722 2 g of choline/kg of diet (Research diets, D12492), a high-choline HFD containing 17 g of
723 choline/kg of diet (Research diets, D16100401), a HC-HFD containing 1% of DMB or a HC-
724 HFD combined with a cocktail of antibiotics (0.5 g/L vancomycin hydrochloride, 1 g/L
725 neomycin trisulfate, 1 g/L metronidazole, 1 g/L ampicillin sodium) in drinking bottles (n=6-
726 10 per group) for 8 weeks (see diet formulations in **Supplementary Table 7**). Mice then
727 were killed by decapitation and organs were dissected and weighed.
728

729 *Irak4*$^{-/-}$ mice. *Irak4*$^{-/-}$ mice on C57BL/6J background as already described[38,45] were bred with
730 C57BL/6J mice (The Jackson Laboratory), and the F1 offspring were subsequently bred to
731 produce *Irak4*$^{-/-}$ mice and WT littermate used for this study. Mice were breaded and
732 genotyped at animal facility of University of Ottawa Heart Institute. The following primers
733 were used for genotyping. Irak4 KO 5'-tga atg gaa gga ttg gag cta cgg ggg t -3'; Irak4 common
734 5'- gaa cac gct ccc agg tct ctt tcc aac; and Irak4 WT 5'- tct tct acc tga aat atg aaa gat tcc t -3'.
735 The PCR reaction were run at 94 ^{o}C 60s, 60 C 60s, 72 C 60s for 40 cycles. 10-12 weeks old mice
736 were feed with HFD for eight weeks and were killed by decapitation and organ were dissected
737 and weighed at the end of the study.
738
739 *Chronic TMA and PF06650833 treatment in LC-HFD-fed mice*. Five-week-old C57BL/6J mice
740 (Charles River) were housed a week before experiment in a controlled environment. Mice
741 were housed under a 12 h–12 h light–dark cycle. At day 0, the 10-week-old mice were
742 anaesthetised with isoflurane (ForeneH, Abbott). Mini-osmotic pumps were implanted
743 subcutaneously (Model 2006, Alzet) (flow rate: 0.15 mL/h, total filling volume: 200 mL,
744 delivery duration: 42 days) as previously described[65]. The osmotic mini-pump contains
745 either vehicle or TMA (0.1 mM in circulation) or PF06650833 (50 nM in circulation). After six
746 weeks of metabolite treatment, mice were killed by decapitation and organs were dissected
747 and weighed.
748
749 Septic shock mouse model. Six-week-old male mice in a C57BL/6J background were
750 purchased from Charles River (Calco, Italy) and maintained in a controlled environment for 2
751 weeks to acclimate them to local conditions. Animal experiment protocol was approved by
752 local and national committees in charge (Tor Vergata University Institutional Animal Care
753 and Use Committee and Ministry of Health, license no. 265/2019-PR) and conducted in
754 accordance with accepted standard of humane animal care. Mice were intraperitoneally
755 injected with 59mg/kg TMA (Sigma Cat.No. 72761) (treatment group, n=7), or PBS alone
756 (control group, n=6) 30 minutes before LPS injection [30 mg/kg of LPS (Sigma Cat.No. L2630)
757 in sterile PBS by intraperitoneal injection]. The survival of the mice was monitored every 4 h
758 for 36 h.
759
760 **Physiological phenotyping.**

761 After 4 weeks of treatment an ipGTT test (2 g/kg) was performed in conscious mice
762 following an overnight fast. Blood was collected from the tail vein before glucose injection
763 and 30, 60, 90 and 120 min afterwards. Blood glucose levels were determined using an
764 Accu-Check® Performa (Roche Diagnostics, Meylan, France). Additional blood samples were
765 collected at baseline and 30 min after glucose injection in Microvette® CB 300 Lithium
766 Heparin (Sarstedt, Marnay, France). Plasma was separated by centrifugation and stored at -
767 80 °C until insulin radioimmunoassay. Circulating insulin levels were determined using
768 Insulin ELISA kits (Mercodia, Uppsala, Sweden). The Matsuda insulin sensitivity index was
769 calculated as previously published[31].
770 After 5 weeks, we performed an ITT. 5-hour-fasted mice were injected intraperitoneally
771 with insulin (0.75 mU/g, Actrapid, Novo Nordisk). Blood glucose levels were measured
772 immediately before and 15, 30, 45, 60, 90 and 120 min after insulin injection with a
773 standard glucose meter (Accu-Check, Roche, Basel, Switzerland) on the tip of the tail vein.
774
775 **Gene expression.**
776 Groups of 6 mice showing consistent pathophysiological profiles in response to CHD or HFD
777 treatment were selected for microarray analysis performed as previously described[64] and
778 data were deposited in ArrayExpress under accession number E-MEXP-1755. The
779 Bioconductor[66] package Limma[67] was used to generate the list of differentially expressed
780 genes. Gene ontology was implemented using Enrichr[68] and signalling pathway impact
781 analysis using SPIA[69].
782 For qPCR analysis, total RNA was prepared from tissues using TriPure reagent (Roche).
783 Quantification and integrity analysis of total RNA were performed by analysing 1 µL of each
784 sample in an Agilent 2100 Bioanalyzer (Agilent RNA 6000 Nano Kit, Agilent). cDNA was
785 prepared by reverse transcription of 1 mg total RNA using a Reverse Transcription System
786 kit (Promega). Real-time PCR was performed with the StepOnePlus real-time PCR system
787 and software (Applied Biosystems) using Mesa Fast qPCR (Eurogentec) for detection
788 according to the manufacturer's instructions. RPL19 RNA was chosen as the housekeeping
789 gene. All samples were performed in duplicate in a single 96-well reaction plate and data
790 were analysed according to the 2_DDCT method. The identity and purity of the amplified
791 product were assessed by melting curve analysis at the end of amplification. The primer
792 sequences for the targeted mouse genes are: SAA1 forward CAT-TTG-TTC-ACG-AGG-CTT-

793 TCC, SAA1 reverse GTT-TTT-CCA-GTT-AGC-TTC-CTT-CAT-GT, SAA2 forward GGG-GTC-TGG-
794 GCT-TCC-CAT-CT, SAA2 reverse CCA-TTC-TGA-AAC-CCT-TGT-GG, SAA3 forward CGC-AGC-
795 ACG-AGC-AGG-AT, SAA3 reverse CCA-GGA-TCA-AGA-TGC-AAA-GAA-TG as reported[70]. Q-RT-
796 PCR assays were performed in a single batch with the personnel blinded to treatment
797 groups.
798
799 **Circulating cytokine quantification.**
800 Circulating cytokines were quantified using MSD V-PLEX Plus Proinflammatory Panel 1 kit.
801 Plasma samples were diluted two times in diluent provided and the experiment was
802 processed as requested by the manufacturer and read on a SECTOR imager 2400. Cytokine
803 assays were performed in a single batch with the personnel blinded to treatment groups.
804
805 **Western-blotting.**
806 Western blot analyses were performed as described previously[71]. To analyze the insulin
807 signaling pathway, mice were allocated to either a saline-injected subgroup or an insulin-
808 injected subgroup so that both subgroups were matched in terms of BW and fat mass. They
809 then received 1 mU insulin/g BW (Actrapid; Novo Nordisk A/S, Denmark) or an equal volume
810 of saline solution. Three minutes after injection, mice were killed and liver was harvested.
811 30 mg of liver were homogenized in 680 µL of RIPA buffer containing a cocktail of protease
812 and phosphatase inhibitors. The homogenate was then centrifuged at 12,000 ***g*** for 20 min at
813 4 °C. Equal amounts of proteins were separated by SDS–PAGE and transferred to
814 nitrocellulose membranes. Membranes were incubated overnight at 4 °C with antibodies
815 diluted in Tris-buffered saline Tween-20 containing 1% bovine serum albumin: p-Akt Ser473
816 (1:1,000; #4060, Cell Signaling), Total Akt (1:1000 ,#9272S, Cell Signalling), p-NF-κB (1:3000,
817 #ab86299, AbCam), Total NF- κB p65 (1:3000, #8242, Cell Signalling). Insulin-induced
818 pAkt/total Akt corresponds to the ratio between pAkt/Akt in insulin treated mice and
819 pAkt/Akt in saline treated mice. For these western blots, the membranes were stripped and
820 re-probed with a β-actin antibody as a loading control.
821
822 **^{1}H-NMR spectroscopy and multivariate statistics.**
823 Mouse urine and plasma samples were prepared and measured on a spectrometer (Bruker)
824 operating at 600.22 MHz ^{1}H frequency; full resolution ^{1}H-NMR spectra were then processed

825 and analysed using orthogonal partial least square discriminant analysis (O-PLS-DA) as
826 described previously[13]. Variance component analysis was performed as described
827 previously[72]. ^{1}H-NMR profiling was performed in a single batch with the personnel blinded
828 to treatment groups. The O-PLS-DA model was validated using 10,000 random permutations
829 of the original class membership variable to explain (i.e. diets, treatments or genotypes), as
830 described previously[72].
831
832 **Plasma methylamine quantification by UPLC-MS/MS.**
833 Methylamines were quantified as previously described[29,30]. Plasma samples (20 µL) were
834 spiked with 10 µL Internal Standard (IS) solution ($^{13}C_3$/^{15}N-TMA, d_9-TMAO, d_4-choline, d_3-
835 carnitine and d_9-betaine in water; 1 mg/L) and 45 µL of ethyl 2-bromoacetate solution (15
836 g/L ethyl 2-bromoacetate, 1% NH_4OH in acetonitrile) were added to derivatize
837 methylamines (TMA and $^{13}C_3$/^{15}N-TMA) to their ethoxy-analogues, completed after 30 min
838 at room temperature. Methylamines were derivatised with ethyl bromoacetate to increase
839 its sensitivity (the underivatized form was giving low response to the mass spectrometer
840 due to its low molecular weight) and enhance its chromatographic performance. 935 µL of
841 protein/lipid precipitation solution (94% acetonitrile/5% water/1% formic acid) was added;
842 samples were centrifuged for 20 min (4°C, 20,000 ***g***) and were transferred to UPLC-
843 autosampler vials. Sample injections (10 µL loop) were performed on a Waters Acquity
844 UPLC-Xevo TQ-S UPLC-MS/MS system equipped with an Acquity BEH HILIC (2.1 × 100 mm,
845 1.7 µm) chromatographic column. An isocratic elution was applied with 10 mM ammonium
846 formate in 95:5 (v/v) acetronitrile:water for 14 min at 500 µL/min and 50 °C. Positive
847 electrospray (ESI+) was used as ionization source and mass spectrometer parameters were
848 set as follows: capillary, cone and source offset voltages at 500, 93 and 50 V, respectively,
849 desolvation temperature at 600 °C, desolvation/cone/nebulizer gases were high-purity
850 nitrogen at 1000 L/hr, 150 L/hr and 7 bar, respectively. Collision gas was high-purity argon.
851 Mass spectrometer was operated in multiple reactions monitoring (MRM) mode. The
852 monitored transitions were the following: for derivatized-TMA, +146 -> +118/59 *m/z* (23/27
853 V); for derivatised-$^{13}C_3$/^{15}N-TMA, +150 -> +63 (27V); for TMAO, +76 -> +59/58 *m/z* (12/13 V);
854 for d_9-TMAO, +85 -> +68 *m/z* (18 V); for choline, +104-> +60/45 *m/z* (14/16 V); for d_4-
855 choline, +108 -> +60 *m/z* (15 V); for γ-butyrobetaine, +146 -> +60/87 *m/z* (12/12 V); for

856 carnitine, +162 -> +103/60 *m/z* (16/14 V); for d_3-carnitine, +165 -> +103 *m/z* (16 V); for
857 betaine, +118 -> +59/58 *m/z* (16/16 V); for d_9-betaine, +127 -> +68 *m/z* (16 V).
858
859 **Kinome screen, K_d.**
860 TMA was assessed using KdELECT screening service (DiscoveRx) as described previously[35,36].
861 This technique is based on a competition-binding assay that quantitatively measures the
862 ability of a compound to compete with an immobilized, active-site-directed ligand. The
863 assay consists of DNA-tagged kinase, immobilized ligand, and the potent inhibitor. The
864 ability of TMA to compete with the immobilized ligand was measured by quantitative PCR of
865 the DNA tag. The binding constant (K_d) was then calculated from duplicate 11-point dose–
866 response curve. Kinase interaction tree plots were generated using TREEspot™ Software
867 Tool and reprinted with permission from KINOMEscan®, a division of DiscoveRx Corporation,
868 © Discoverx corporation 2015.
869
870 **Kinase activity assays.**
871 The TMA IC_{50} on IRAK4 was determined using Kinexus kinase-inhibitor activity profiling
872 service (Kinexus, Vancouver, Canada). Protein kinase assays (in duplicate) were performed
873 at ambient temperature for 30 min in a final volume of 25 µL according to the following
874 assay reaction recipe:
875 ***Component 1***. 5 µl of diluted active IRAK4 target (recombinant, full length, expressed by
876 baculovirus in Sf9 insect cells with an GST tag (SignalChem Catalogue 112 – 10G); ~10-50 nM
877 final concentration in the assay).
878 ***Component 2***. 5 µl of stock solution of substrate (Myelin Basic Protein 1mg/ml diluted in
879 H_2O).
880 ***Component 3***. 5 µl of kinase assay buffer (25 mM MOPS, pH 7.2, 12.5 mM β-glycerol-
881 phosphate, 25 mM $MgCl_2$, 5 mM EGTA, 2 mM EDTA, 0.25 mM DTT, added just prior to assay
882 initiation).
883 ***Component 4***. 5 µl of compound (various concentration as indicated) or 10% DMSO for
884 blank.
885 ***Component 5***. 5 µl of ^{32}P-ATP (250 µM stock solution, 0.8 µCi, Perkin Elmer).
886 The assay was initiated by the addition of ^{32}P-ATP and the reaction mixture incubated at
887 ambient temperature for 30 min. After the incubation period, the assay was terminated by

888 spotting 10 µL of the reaction mixture onto Multiscreen phosphocellulose P81 plate. The
889 Multiscreen phosphocellulose P81 plate was washed 3 times for approximately 15 min each
890 in a 1% phosphoric acid solution. The radioactivity on the P81 plate was counted in the
891 presence of scintillation fluid in a Trilux scintillation counter. Blank control was set up that
892 included all the assay components except the addition of Myelin Basic Protein (replaced
893 with equal volume of assay dilution buffer). The corrected activity for IRAK4 target was
894 determined by removing the blank control value.
895
896 **Reagents.**
897 Glutamine (Glutamax, 35050061, Life Technologies), Fetal bovine serum (Life Technologies),
898 crystal violet (C6158) and Trimethylamine (W324108) were from Sigma-Aldrich. Mouse IL-6
899 Quantikine ELISA kits (M6000B, R&D system), RNeasy Micro Kit (Qiagen). SuperScript II
900 Reverse Transcriptase, IL6 Taqman probe Hs00174131_m1 and FAST master mix
901 (Invitrogen). High Fat Diet (Special Diets Services) and Low Fat Diet (B & K Universal) were
902 specifically formulated in[12]. Control Diet (D12450K; Research diet), LC-HFD (60% kcal fat and
903 20% kcal carbohydrates, D12492, Research diet), HC-HFD (60% kcal fat and 20% kcal
904 carbohydrates with 17 g of choline/kg, D16100401i, Research diet). Mouse Insulin ELISA (10-
905 1249-01, Mercodia). Isoflurane (10014451, Forene, Abbott). TriPure reagent (1667165,
906 Roche). Reverse Transcription System kit (A3500, Promega). Mesa Fast qPCR (CS-CKIT-PROD,
907 Eurogentec). MSD V-PLEX Plus Proinflammatory Panel 1 kit (K15048G Meso Scale
908 Diagnostics).
909
910 **Statistics.**
911 Potential outliers were identified by a Grubbs test. For statistical comparisons between
912 study groups, normality was tested using D'agostino-Pearson omnibus normality test, then
913 one-way ANOVA was used, followed by Tukey's *post hoc* testing when data were normally
914 distributed, otherwise groups were compared using the two-tailed Mann-Whitney test ($P <$
915 0.05 considered to be statistically significant). Data are displayed as mean ± s.e.m in all
916 figures. All cell culture experiments included at least three biological replicates (as indicated
917 in figure legends). All animal cohorts included at least five animals in each study group (as
918 indicated in figure legends) and animals were randomized to treatment groups.

919 **Figure Legends.**

920

921 **Figure 1. Choline supplementation improves glucose homeostasis and inflammation after**
922 **5 months of HFD.**

923 Male mice were weaned at 3 weeks and fed a CHD diet, before being randomly assigned to
924 CHD group (n=68) or HFD (n=47) groups and monitored at 5 months of age. Effect of HFD-
925 feeding on (**a**) glucose tolerance test (GTT). (**b**) Volcano plot of differentially expressed liver
926 genes, highlighting that *Saa1* and *Saa2* are down-regulated in HFD after 4 months of HFD.
927 Red dots, significantly (FDR < 0.1) upregulated genes; blue dots, significantly (FDR < 0.1)
928 downregulated genes. (**c**) Metabolic signature of diet on O-PLS model coefficient plot; line
929 plot corresponds to covariance and the color-scale represents proportion of variance
930 explained. (**d**) Assessment of the contribution of factors diet and age on choline, TMA and
931 TMAO by O-PLS variance components analysis. 5-week-old C57BL/6J mice were fed a CHD
932 diet, a low-choline HFD or a low-choline HFD supplemented with choline (n=10) and were
933 phenotyped after 5 months. (**e**) Plasma glucose concentration during an ipGTT. (**f**) Area
934 under the curve of the plasma glucose concentration during an ipGTT. (**g**) Body weight (BW)
935 measured after 5 months of diet. (**h-j**) Quantification of circulating cytokines: IL6 (**h**), TNFα
936 (**i**) and IL1β (**j**). (**k**) Scores plot from a cross-validated O-PLS-DA model segregating the three
937 groups of mice according to diet based on isotopic quantification of methylamines by UPLC-
938 MS/MS, each component's explained variance is shown in parenthesis. (**l**) Empirical
939 assessment of the significance of O-PLS goodness-of-fit parameters by generating a null
940 distribution with 10,000 random permutations. (**m-n**) Quantification of circulating TMA (**m**)
941 and TMAO (**n**) by UPLC-MS/MS. Data are means ± s.e.m. One-way ANOVA followed by
942 Tukey's *post hoc* tests (superscript letters for factor levels P<0.05) on log-transformed data
943 except (**k&l**).

944

945 **Figure 2. Choline supplementation corrects HFD adverse effects on glucose homeostasis,**
946 **insulin sensitivity and inflammation after 8 weeks of diet.**

947 Five-week-old C57BL/6J mice were fed a CHD diet, a low-choline HFD or a low-choline HFD
948 supplemented with choline (n = 10) and were phenotyped after 8 weeks. (**a**) Plasma glucose
949 concentration during an ipGTT. (**b**) Area under the curve of the plasma glucose
950 concentration during an ipGTT. (**c**) Matsuda insulin sensitivity index calculated from the

951 ipGTT. (**d**) Body weight measured periodically during 8 weeks of diet. (**e**) Plasma glucose
952 concentration during an ipITT. (**f**) Area under the curve of the plasma glucose concentration
953 during an ipITT. (**g-j**) Western-blot analysis of liver Akt phosphorylation (**g-h**) and NF-kB
954 phosphorylation (**i-j**). (**k-m**) Expression of hepatic acute phase inflammation proteins
955 markers *Saa1* (**k**), *Saa2* (**l**) and *Saa3* (**m**). Data are means ± s.e.m. (**c**, **d**, **f**, **h-m**) One-way
956 ANOVA followed by Tukey's *post hoc* tests (superscript letters for factor levels $P<0.05$) on
957 log-transformed data. (**a**, **b**, **e**) Non-parametric two-sided Mann-Whitney test was used for
958 each timepoint, significance comparison signs are as follow: *=CHD vs LC-HFD, $=LC-HFD vs
959 HC-HFD and #=CHD vs HC-HFD.
960
961 **Figure 3. Blocking TMA production from choline cancels metabolic benefits from choline**
962 **supplementation and chronic TMA chronic treatment mimics it.**
963 (**a-e**) Five-week-old C57BL/6J mice were fed a low-choline HFD or a low-choline HFD
964 supplemented with choline (n = 10). Two strategies were used in parallel to block TMA
965 production from choline by the gut microbiota using either 1% DMB in the diet or an
966 antibiotic treatment. (**a**) Plasma glucose concentration during an ipGTT. (**b**) Area under the
967 curve of the plasma glucose concentration during an ipGTT. (**c**) Matsuda insulin sensitivity
968 index calculated from the ipGTT. (**d-e**) Western-blot analysis of liver Akt phosphorylation. (**f-**
969 **l**) Mice were weaned at 3 weeks and fed a low-choline HFD before being fitted with osmotic
970 minipumps delivering a chronic circulating dose of TMA (0.1 mM) for 6 weeks (n = 9 saline
971 HFD, n = 8 TMA HFD). (**f**) Plasma glucose concentration during an ipGTT. (**g**) Area under the
972 curve of the plasma glucose concentration during an ipGTT. (**h**) Matsuda insulin sensitivity
973 index calculated from the ipGTT. (**i**) Quantification of circulating IL6. (**j-l**) Expression of
974 hepatic acute-phase inflammation protein markers *Saa1* (**j**), *Saa2* (**k**) and *Saa3* (**l**). Data are
975 means ± s.e.m. Results were assessed by one-way analysis of variance followed by Tukey's
976 *post hoc* tests (superscript letters for factor levels $P<0.05$) on log-transformed data.
977
978 **Figure 4. TMA inhibits IRAK4 and rescues LPS-induced TLR4-mediated pro-inflammatory**
979 **response.**
980 (**a**) Kinome screen for a single dose of TMA (0.1 mM) against 456 kinases. (**b**) Functional
981 characterization of the inhibition of IRAK4 by TMA. IRAK4 phosphorylation activity was
982 determined in presence of various concentration of TMA and resulted in an IC_{50} of 3.4 µM.

983 TMA preincubation (100 µM, for 30 min) suppresses LPS-induced (1 µg/ml, 4h) IL6 (**c**) and
984 TNFα (**d**) release by human PBMCs. The values of the unstimulated controls were arbitrarily
985 set to 1. *<0.05 vs LPS-stimulated control. (**e**) TMA (100µM) or the IRAK4 specific inhibitor
986 PF06650833 (PF; 50nM) do not inhibit TNFα secretion from human PBMCs after 4h
987 stimulation with PMA (50ng/ml) and ionomycin (1µg/ml). (**f**) Impact of TMA pre-treatment
988 (100 µM, 30 min) on human PBMCs' ^{Thr209}IRAK1/IRAK1 phosporylation upon LPS (1 µg/ml)
989 stimulation for the indicated times. (**g**) Human PBMCs were pre-treated (for 30 min) with
990 the indicated concentrations of TMA and ^{Thr209}IRAK1/IRAK1 phosporylation was assessed
991 after 10 min of LPS (1 µg/ml) challenge. The time- (**h**) and dose-dependent (**i**) effect of TMA
992 on phosphorylation of ^{Ser536}NF-κBp65/NF-κBp65 of human PBMCs stimulated with LPS (1
993 µg/ml) was assessed as in (**f**) and (**g**). For (**f-i**), the control value was arbitrarily set to one
994 and statistical significance (*<0.05) was assessed with unpaired Student's *t* test. (**j**) 24-hour
995 survival curve of mice challenged with a lethal dose of LPS (30 mg/kg) that received a single
996 dose of TMA (59mg/kg, red line), or vehicle (black line). The kinases covered by the kinome
997 scan assay are visualised using a phylogenetic layout. Preliminary positive hits with potential
998 binding >35 % vs control (DMSO) are represented by a red dot whilst non-binding kinases
999 are represented by a green dot. Kinase group names: TK, Tyrosine Kinases; TKL, Tyrosine
1000 Kinase-like; STE, STE kinase group; CK1, Cell Kinase 1; AGC, Protein kinase A, G and C
1001 families; CAMK, Calcium and Calmodulin-regulated kinases; CMGC, CMGC kinase group.
1002 Data are means ± s.e.m.
1003
1004 **Figure 5. IRAK4 deficiency corrects IGT and pro-inflammatory response after 8 weeks of**
1005 **low choline HFD feeding in C57BL/6 mice and a chemical inhibitor of IRAK4 mimics the**
1006 **effects on glucose homeostasis.** (**a-h**) 5-week-old *Irak4*$^{-/-}$ mice and wild-type (WT)
1007 littermates were fed a low-choline HFD (10 WT HFD and 8 *Irak4*$^{-/-}$ HFD) and were
1008 phenotyped after 8 weeks. (**a**) Plasma glucose concentration during an ipGTT. (**b**) Area
1009 under the curve of the plasma glucose concentration during an ipGTT. (**c-e**) Circulating
1010 cytokines (**c**) IL6, (**d**) TNFα, (**e**) IL1β. (**f-h**) Liver mRNA expressions for *Saa1* (**f**), *Saa2* (**g**) and
1011 *Saa3* (**h**) genes. (**i-n**) Mice were weaned at 3 weeks and fed a low-choline HFD before being
1012 fitted with osmotic minipumps delivering a chronic circulating dose of PF06650833 (50 nM)
1013 for 6 weeks. (**i**) Plasma glucose concentration during an ipGTT. (**j**) Area under the curve of
1014 the plasma glucose concentration during an ipGTT. (**k**) Plasma glucose concentration during

1015 an ipITT. (**l**) Area under the curve of the plasma glucose concentration during an ipITT. (**m-n**)
1016 Western-blot analysis of liver Akt phosphorylation. Data are means ± s.e.m. Student's *t* test
1017 ($P<0.05$) on log-transformed data.
1018
1019 **Fig. 6. Overview of effects of IRAK4 inhibition by TMA on metabolic response to HFD.** TMA
1020 is synthesized from dietary choline (1) by the gut microbiota (2) and specifically inhibits
1021 IRAK4 activity (3). This inhibition blunts the TLR signalling pathway (induced by LPS and
1022 saturated free fatty acids) leading to an improvement of metabolic response to HFD (e.g.
1023 glucose homeostasis).
1024
1025

1026 **Extended Data Figure Legends**

1027

1028 **Extended Data Figure 1. C57BL/6 mice fed HFD display low acute-phase gene expression in**
1029 **liver paralleled by high TMA excretion.** Male mice were weaned at 3 weeks and fed CHD,
1030 before being randomly assigned to CHD group (n=270) or HFD (n=202) groups and
1031 monitored at 2 (72 CHD and 64 HFD), 3 (84 CHD and 57 HFD), 5 (68 CHD and 47 HFD) and 7
1032 months (46 CHD and 34 HFD). (**a-b**) Effect of HFD-feeding on physiological parameters. (**a**)
1033 Body weight (BW) and (**b**) cumulative glycemia during GTT (AUC). (**c**) Heatmap of
1034 significantly (FDR < 0.1) differentially expressed liver genes after 4 months of HFD. (**d**) ^{1}H-
1035 NMR-based metabotyping scores plot from a cross-validated O-PLS-DA model segregating
1036 the eight groups of mice according to both diet and age. (**e**) Empirical assessment of the
1037 significance of O-PLS goodness-of-fit parameters by generating a null distribution with
1038 10,000 random permutations. Data are means ± s.e.m. Two-sided Mann-Whitney test (*P <
1039 0.05 vs control). For the O-PLS-DA permutation test, the horizontal axis corresponds to the
1040 correlation between the original class membership variable (single dots on the right) and
1041 the randomly permuted class membership vectors (no longer correlated with the original
1042 class membership) (swarm of permutated models on the left). The *y* axis corresponds to
1043 goodness-of-fit parameter R^2 (in green) derived for each O-PLS-DA model and the goodness-
1044 of-prediction parameter Q^2 (in blue) derived by 7-fold cross-validation of each O-PLS-DA
1045 model. The R^2 and Q^2 parameters obtained from the original model in the top right corner
1046 are outside the confidence interval of the 10,000 randomly permuted models and therefore
1047 confirming the significance of the fitness and prediction capacity of the original O-PLS-DA
1048 model.

1049

1050 **Extended Data Figure 2. Pathway analysis for hepatic significant genes.** (**a**) Gene ontology
1051 analysis for down- and up-regulated HFD-responsive genes. (**b**) Signaling pathway impact
1052 analysis for HFD-responsive genes. Pathways respectively on the right-hand side of the red
1053 and blue curves are significant after Bonferroni correction of the global p-values (pG)
1054 obtained by combining the pPERT and pNDE using the normal inversion method, and
1055 significant after a FDR correction of pG. Significant KEGG pathways: 04141, Protein
1056 processing in the endoplasmic reticulum; 04710, Circadian rhythm; 04152, AMPK signaling
1057 pathway.

1058

1059 **Extended Data Figure 3. Choline supplementation corrects HFD adverse effects and**
1060 **associated methylamine measurements.** (**a**) Food intake measured on the three tested
1061 diets (CHD, LC-HFD and HC-HFD). (**b-c**) Western blot analysis of liver NF-kB phosphorylation
1062 state between LC-HFD and HC-HFD. (**d**) Plasma sample chromatogram for the simultaneous
1063 detection of TMA, TMAO, choline, γ-butyrobetaine, carnitine, betaine and their isotopically
1064 labelled analogues. (**e**) Principal Component Analysis Biplot of plasma methylamine
1065 quantifications by UPLC/MS-MS from mice fed CHD, LC-HFD and HC-HFD, each component's
1066 explained variance is shown in parenthesis. Data are means ± s.e.m. Two-sided Mann-
1067 Whitney test (*P < 0.05 vs control).

1068

1069 **Extended Data Figure 4. Modulation of TMA production and effects.** (**a-d**) Confirmation of
1070 blockage of production of TMA (**a**, **c**) and TMAO (**b**, **d**) by 1% DMB measured in plasma (**a-b**)
1071 and urine (**c-d**). (**e**) Body weight monitoring during the whole experiment of mice fed a LC-
1072 HFD and a HC-HFD supplemented or not with DMB or treated with antibiotics. (**f**) Plasma
1073 insulin concentration during GTT at 0, 30 and 120 min post glucose injection. (**g**) Body
1074 weight monitoring during the whole experiment of mice fed a LC-HFD and chronically
1075 treated with TMA. (**h**) Plasma insulin concentration during GTT at 0, 30 and 120 min post
1076 glucose injection. Data are means ± s.e.m. Two-sided Mann-Whitney test (*P < 0.05 vs LC-
1077 HFD control).

1078

1079 **Extended Data Figure 5. TMA does not bind with kinases ANKK1, HIPK2, JAK2, and NDR1**
1080 **identified as candidates in the kinome screen, but makes significant contact with IRAK4.**
1081 (**a**) Confirmation of a physical interaction between TMA and IRAK4 using TMA at
1082 concentrations ranging from 0.1 nM to 100 µM, resulting in a dissociation constant (K_d) of
1083 14 nM. (**b-e**) Physical interaction test between TMA and the four hits identified using a
1084 kinome screen, using TMA concentrations ranging from 0.1 nM to 100 µM for (**b**) ANKK1, (**c**)
1085 HIPK2, (**d**) JAK2 and (**e**) NDR1. IRAK4 kinase activity is not significantly inhibited by choline
1086 (**f**), TMAO (**g**) or DMB (**h**), while TMA does not have any inhibitory effect on IRAK-1 kinase
1087 activity (**i**). (**j-k**) Phosphorylation for $^{pThr183/Tyr185}$SAPK/JNK/SAPK/JNK (**j**) and
1088 $^{pThr180/Tyr182}$p38MAPK/p38MAPK (**k**) ratios. Data are means ± s.e.m. One-way ANOVA

followed by Tukey's *post hoc* tests (superscript letters for factor levels $P<0.05$) on log-transformed data.

Extended Data Figure 6. TMA inhibits IRAK4 and suppresses TLR4-mediated pro-inflammatory response in primary human hepatocytes. (**a-d**) Effect of palmitate (PA; 200 µM) administration and TMA pre-treatment (0.1 mM, 30 min) in primary human hepatocytes at 0 and 60 min on $^{pThr345/Ser346}$IRAK4/IRAK4 (**a**), ^{pThr209}IRAK1/IRAK1 (**b**), $^{pSer176/180}$IKKαβ/IKKβ (**c**), ^{pSer536}NF-κBp65/NF-κBp65 (**d**) ratios. *p<0.05 and **p<0.01 *vs* 0 min; †p<0.05 and ††p<0.01 *vs* vehicle; ^{b}p=0.07 *vs* vehicle. Effect of PA (200 µM) administration (4 h) with and without TMA pre-treatment (0.1 mM, 30 min) on IL6 accumulation in hepatocyte media (**e**) and on ^{pSer473}Akt1/Akt1 after insulin stimuli (100 nM, 10min) (**f**). *p<0.05 and **p<0.01 *vs* control-vehicle; †p<0.05 *vs* control-PA.

Extended Data Figure 7. IRAK4 knock-out does not affect body weight while chronic treatment with PF06650833 reduces it in mice fed a low-choline HFD. (**a**) representative agarose gel of PCR products from +/-irak4 and -/-irak4 mice. (**b-c**) Body weight monitoring during the whole experiment of *Irak4*$^{-/-}$ mice (**b**) or PF06650833-treated mice (**c**) fed a LC-HFD.

1121 **Supplementary Tables**

1122

1123 **Supplementary Table 1: Hepatic genes differentially expressed by HFD-feeding.** Hepatic
1124 transcriptomes were analysed using Limma[55] and genes are considered significant if
1125 FDR<0.1.

1126

1127 **Supplementary Table 2: Down-regulated HFD-responsive hepatic pathways.** Gene
1128 ontology analysis was performed using Enrichr[56] and pathways are considered significant if
1129 FDR<0.1.

1130

1131 **Supplementary Table 3: Up-regulated HFD-responsive hepatic genes.** Gene ontology
1132 analysis was performed using Enrichr[56] and pathways are considered significant if FDR<0.1.

1133

1134 **Supplementary Table 4: Hepatic signalling pathways impacted by HFD.** Signalling pathway
1135 impact analysis was performed using SPIA[57] and pathways are considered significant if
1136 pGFWER<0.1.

1137

1138 **Supplementary Table 5. TMA kinome screen.** Screening results for single-dose TMA binding
1139 to 456 kinases. "Percent control" corresponds to the percentage of DNA amplified by qPCR
1140 compared to the control condition. Values below 35 % (in green) are considered as positive
1141 hits.

1142

1143 **Supplementary Table 7. Diet formulations.** Specific fat, protein, carbohydrate and choline
1144 content in regimens formulated by Research Diet are summarized based on per cent w/w
1145 and per cent kcal.

1146 **Online References.**
1147

1148 56. Ahmetaj-Shala, B. *et al*. A bioassay system of autologous human endothelial, smooth
1149 muscle cells, and leukocytes for use in drug discovery, phenotyping, and tissue
1150 engineering. *FASEB J* **34**, 1745-1754 (2020).
1151 57. Latorre, J. *et al.* Decreased lipid metabolism but increased FA biosynthesis are
1152 coupled with changes in liver microRNAs in obese subjects with NAFLD. *Int J Obes*
1153 *(Lond)* **41,** 620–630 (2017).
1154 58. Fearnside, J. F. *et al.* Phylometabonomic patterns of adaptation to high fat diet
1155 feeding in inbred mice. *PLoS ONE* **3,** e1668 (2008).
1156 59. Geurts, L., Muccioli, G. G., Delzenne, N. M. & Cani, P. D. Chronic endocannabinoid
1157 system stimulation induces muscle macrophage and lipid accumulation in type 2
1158 diabetic mice independently of metabolic endotoxaemia. *PLoS ONE* **8,** e55963 (2013).
1159 60. Toye, A. A. *et al.* Subtle metabolic and liver gene transcriptional changes underlie
1160 diet-induced fatty liver susceptibility in insulin-resistant mice. *Diabetologia* **50,** 1867–
1161 1879 (2007).
1162 61. Gentleman, R., Carey, V. J., Huber, W., Irizarry, R. A. & Dudoit, S. *Bioinformatics and*
1163 *Computational Biology Solutions Using R and Bioconductor*. (Springer, 2006).
1164 62. Smyth, G. K. in *… and computational biology solutions using R and …* 397–420
1165 (Springer-Verlag, 2005). doi:10.1007/0-387-29362-0_23
1166 63. Chen, E. Y. *et al.* Enrichr: interactive and collaborative HTML5 gene list enrichment
1167 analysis tool. *BMC Bioinformatics* **14,** 128 (2013).
1168 64. Tarca, A. L. *et al.* A novel signaling pathway impact analysis. *Bioinformatics* **25,** 75–82
1169 (2009).
1170 65. Plovier, H. *et al.* A purified membrane protein from Akkermansia muciniphila or the
1171 pasteurized bacterium improves metabolism in obese and diabetic mice. *Nat. Med.*
1172 **23,** 107–113 (2017).
1173 66. Blaise, B. J. *et al.* Metabotyping of Caenorhabditis elegans reveals latent phenotypes.
1174 *Proc. Natl. Acad. Sci. U.S.A.* **104,** 19808–19812 (2007).

1175

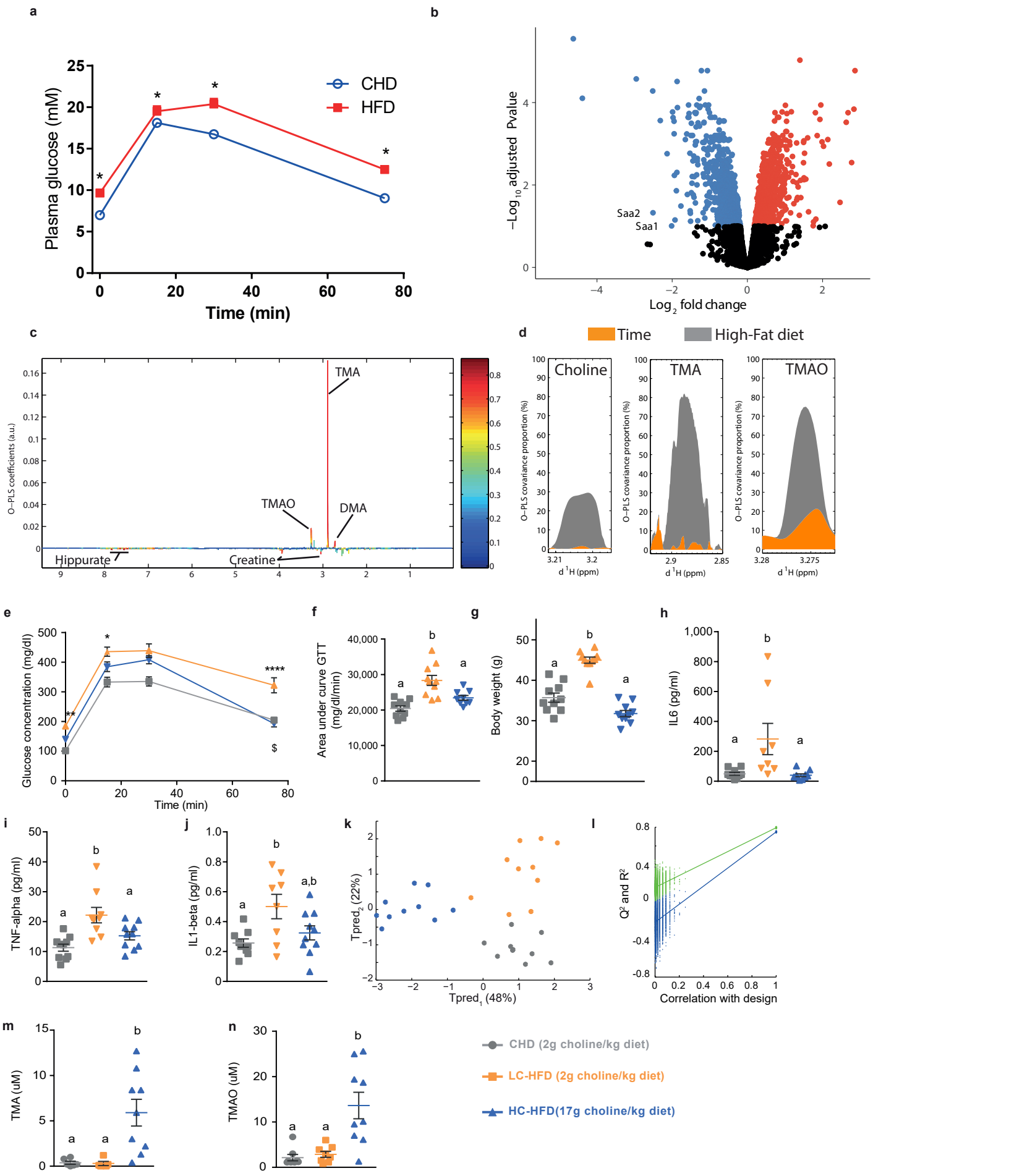
a
Plasma glucose (mM)
Time (min)
CHD
HFD
b
−Log10 adjusted Pvalue
Log2 fold change
Saa2
Saa1
c
O−PLS coefficients (a.u.)
TMA
TMAO
DMA
Hippurate
Creatine
d
Time
High-Fat diet
Choline
TMA
TMAO
O−PLS covariance proportion (%)
d 1H (ppm)
e
Glucose concentration (mg/dl)
Time (min)
f
Area under curve GTT (mg/dl/min)
g
Body weight (g)
h
IL6 (pg/ml)
i
TNF-alpha (pg/ml)
j
IL1-beta (pg/ml)
k
Tpred2 (22%)
Tpred1 (48%)
l
Q2 and R2
Correlation with design
m
TMA (uM)
n
TMAO (uM)
CHD (2g choline/kg diet)
LC-HFD (2g choline/kg diet)
HC-HFD(17g choline/kg diet)

CHD (2g choline/kg diet) LC-HFD (2g choline/kg diet) HC-HFD(17g choline/kg diet)

a
Glucose concentration (mg/dl)
Time (minutes)

b
Area under curve GTT (mg/dL/min)

c
Matsuda insulin sensitivity index

d
Body weight (g)
Time (Days)

e
Glucose concentration (mg/dL)
Time (min)

f
Area under curve ITT (mg/dL/min)

g
CHD LC-HFD HC-HFD
Insulin
70 KDa- Akt
70 KDa- P-Akt (Ser)

i
CHD LC-HFD HC-HFD
MWM
NF-kB p65
NF-kB p65 (pS536)

h
Insulin induced P-Akt^{Ser}/Total Akt (arbitrary units)

j
NF-kB p65 (pS536) / NF-kB p65

k
Liver *Saa1* mRNA (relative expression)

l
Liver *Saa2* mRNA (relative expression)

m
Liver *Saa3* mRNA (relative expression)

2

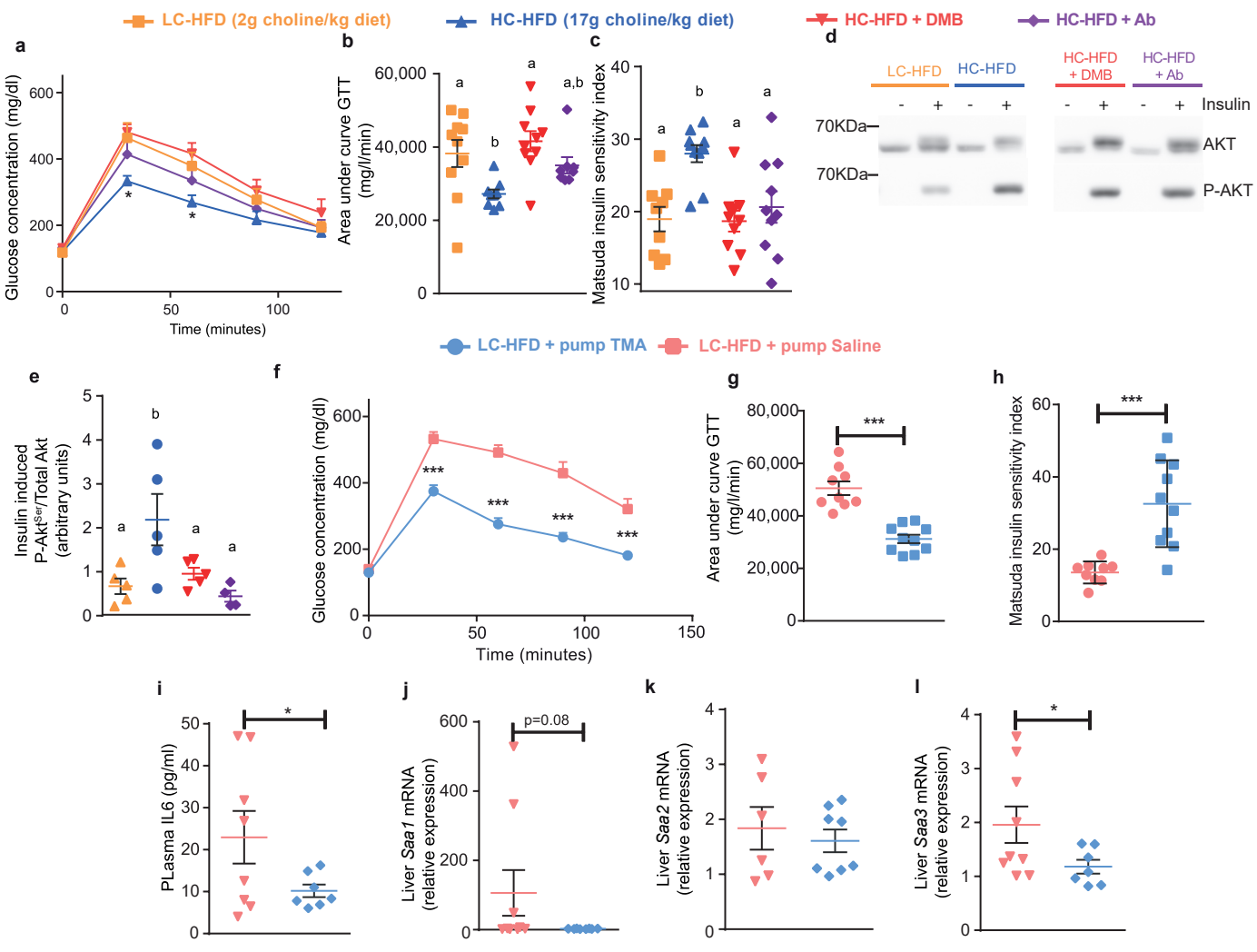
LC-HFD (2g choline/kg diet)
HC-HFD (17g choline/kg diet)
HC-HFD + DMB
HC-HFD + Ab
a
Glucose concentration (mg/dl)
Time (minutes)
b
Area under curve GTT (mg/l/min)
c
Matsuda insulin sensitivity index
d
LC-HFD
HC-HFD
HC-HFD + DMB
HC-HFD + Ab
Insulin
70KDa
AKT
P-AKT
LC-HFD + pump TMA
LC-HFD + pump Saline
e
Insulin induced P-Akt^{Ser}/Total Akt (arbitrary units)
f
Glucose concentration (mg/dl)
Time (minutes)
g
Area under curve GTT (mg/l/min)
h
Matsuda insulin sensitivity index
i
PLasma IL6 (pg/ml)
j
Liver Saa1 mRNA (relative expression)
p=0.08
k
Liver Saa2 mRNA (relative expression)
l
Liver Saa3 mRNA (relative expression)

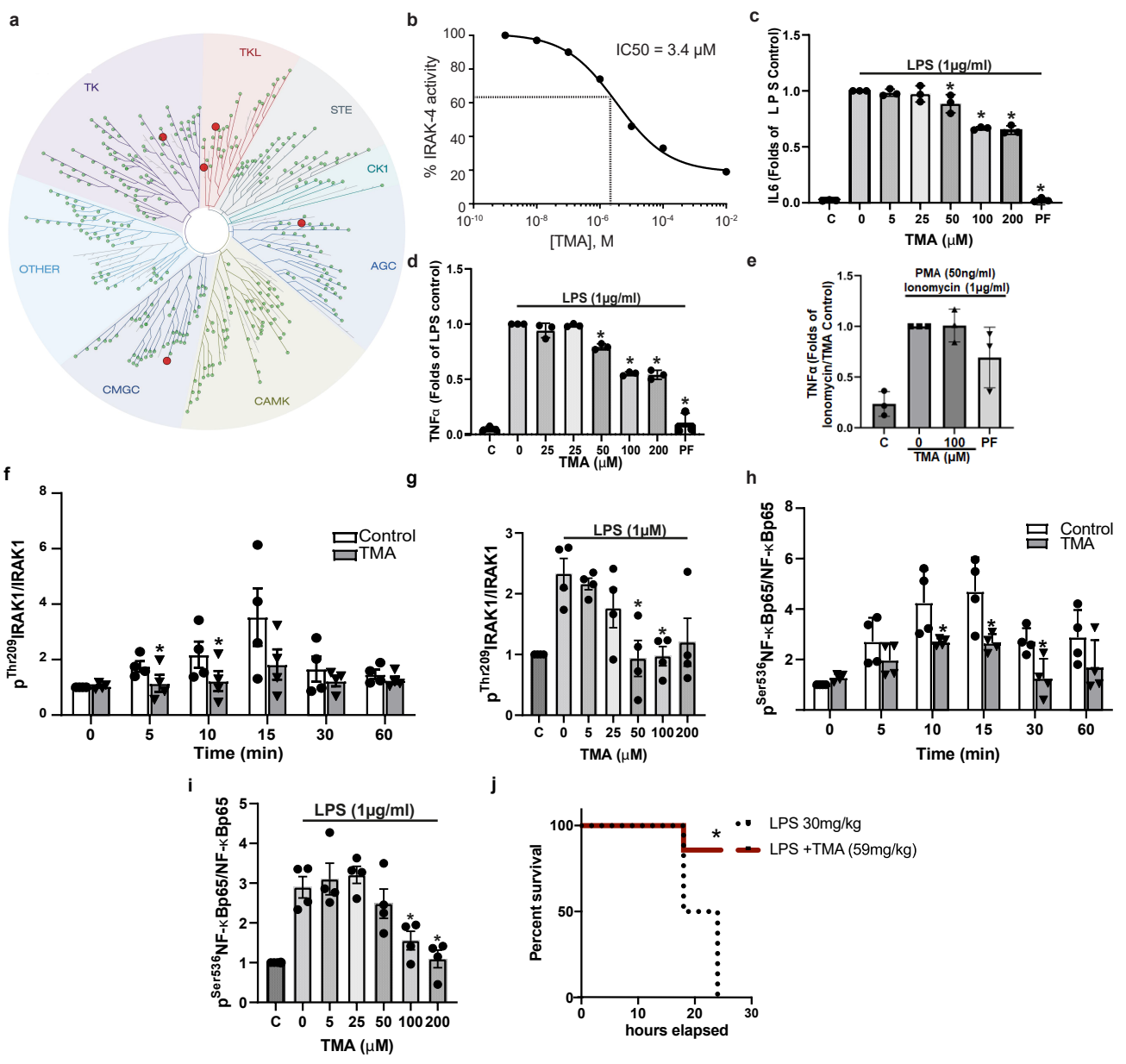
a
TKL
TK
STE
CK1
OTHER
AGC
CMGC
CAMK
b
IC50 = 3.4 μM
% IRAK-4 activity
[TMA], M
c
LPS (1μg/ml)
IL6 (Folds of L P S Control)
C 0 5 25 50 100 200 PF
TMA (μM)
d
LPS (1μg/ml)
TNFα (Folds of LPS control)
C 0 25 25 50 100 200 PF
TMA (μM)
e
PMA (50ng/ml)
Ionomycin (1μg/ml)
TNFα (Folds of Ionomycin/TMA Control)
C 0 100 PF
TMA (μM)
f
Control
TMA
pThr209IRAK1/IRAK1
0 5 10 15 30 60
Time (min)
g
LPS (1μM)
pThr209IRAK1/IRAK1
C 0 5 25 50 100 200
TMA (μM)
h
Control
TMA
pSer536NF-κBp65/NF-κBp65
0 5 10 15 30 60
Time (min)
i
LPS (1μg/ml)
pSer536NF-κBp65/NF-κBp65
C 0 5 25 50 100 200
TMA (μM)
j
LPS 30mg/kg
LPS +TMA (59mg/kg)
Percent survival
hours elapsed

4

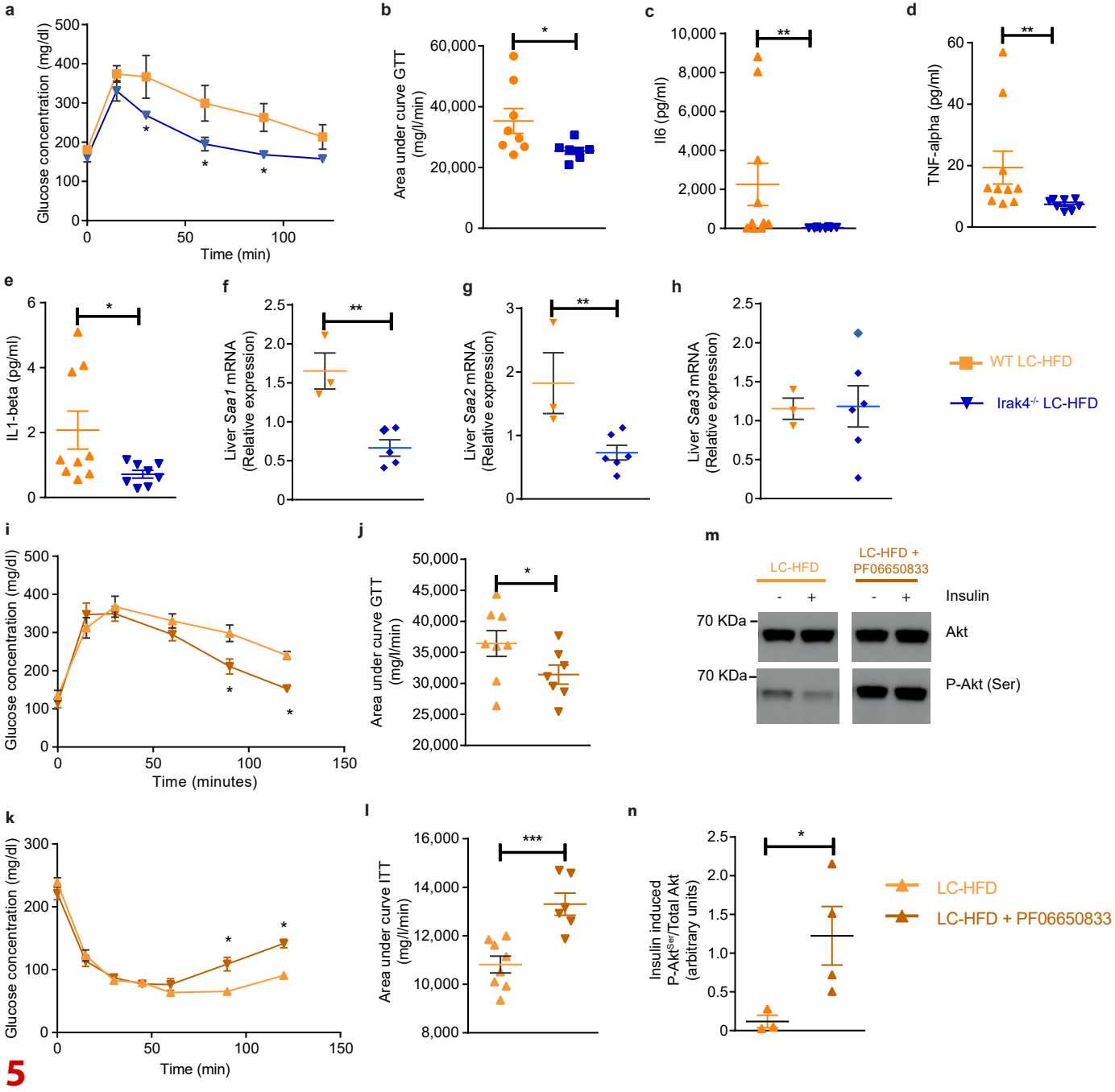
a
Glucose concentration (mg/dl)
Time (min)
b
Area under curve GTT (mg/l/min)
c
Il6 (pg/ml)
d
TNF-alpha (pg/ml)
e
IL1-beta (pg/ml)
f
Liver Saa1 mRNA (Relative expression)
g
Liver Saa2 mRNA (Relative expression)
h
Liver Saa3 mRNA (Relative expression)
WT LC-HFD
Irak4-/- LC-HFD
i
Glucose concentration (mg/dl)
Time (minutes)
j
Area under curve GTT (mg/l/min)
m
LC-HFD
LC-HFD + PF06650833
Insulin
70 KDa
Akt
P-Akt (Ser)
k
Glucose concentration (mg/dl)
Time (min)
l
Area under curve ITT (mg/l/min)
n
Insulin induced P-Akt^Ser/Total Akt (arbitrary units)
LC-HFD
LC-HFD + PF06650833

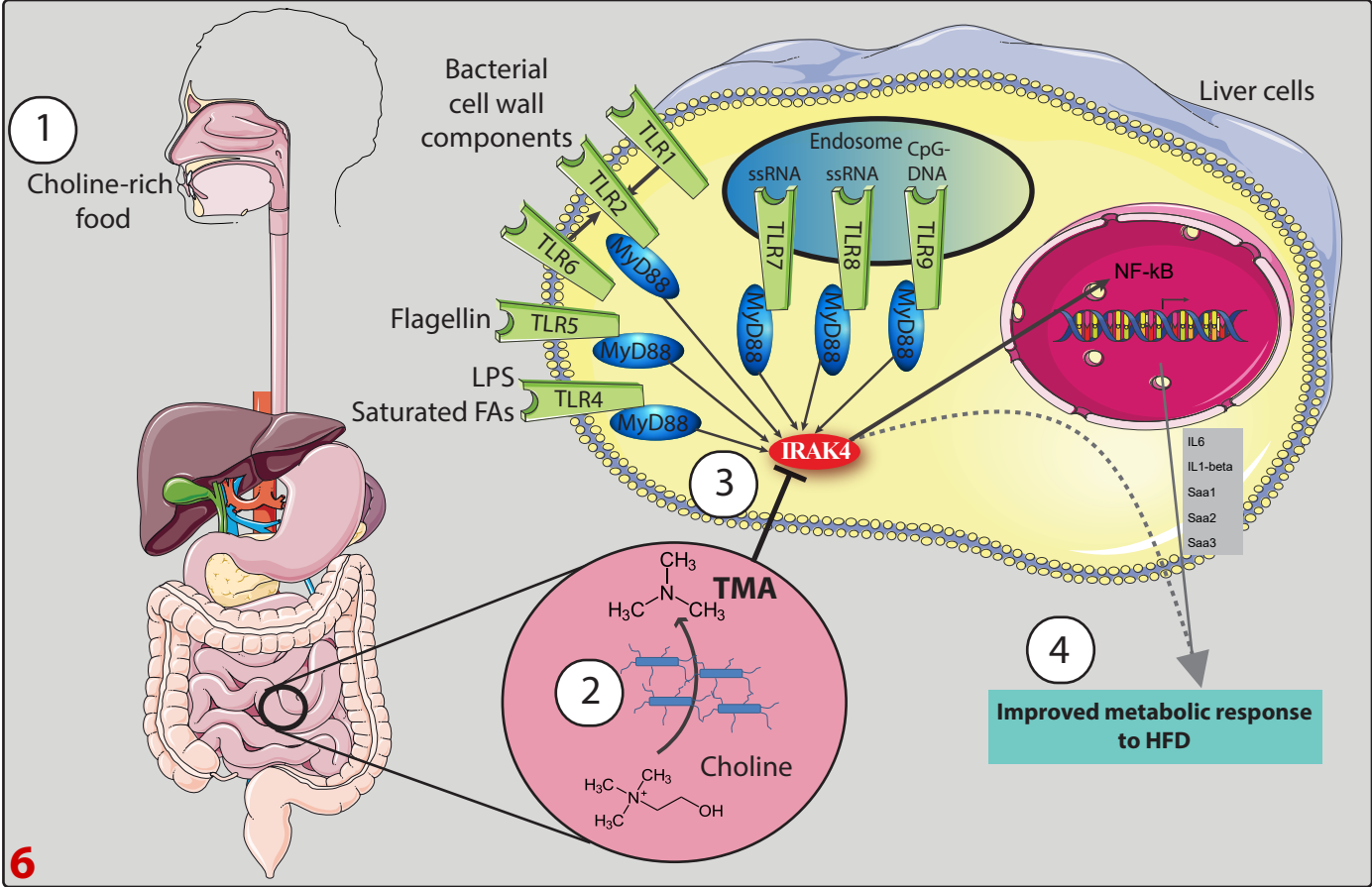
1
Choline-rich food
Bacterial cell wall components
TLR1
TLR2
TLR6
Flagellin
TLR5
LPS
Saturated FAs
TLR4
MyD88
Endosome
ssRNA
ssRNA
CpG-DNA
TLR7
TLR8
TLR9
Liver cells
NF-kB
IRAK4
3
IL6
IL1-beta
Saa1
Saa2
Saa3
TMA
2
Choline
4
Improved metabolic response to HFD
6

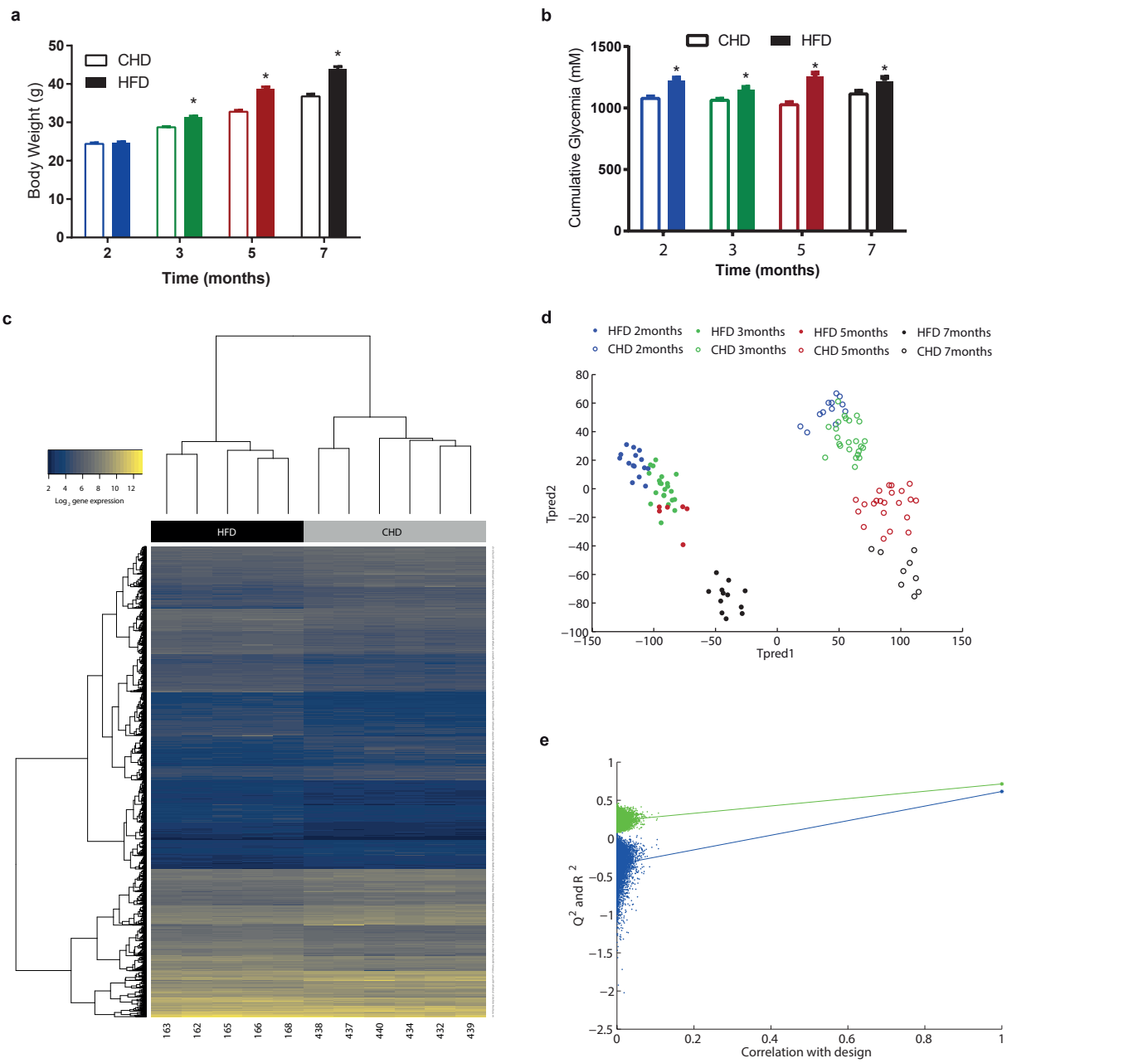
a
CHD
HFD
Body Weight (g)
Time (months)
b
CHD
HFD
Cumulative Glycemia (mM)
Time (months)
c
Log2 gene expression
HFD
CHD
163
162
165
166
168
438
437
440
434
432
439
d
HFD 2months
HFD 3months
HFD 5months
HFD 7months
CHD 2months
CHD 3months
CHD 5months
CHD 7months
Tpred2
Tpred1
e
Q2 and R2
Correlation with design

S1

a

SIGNIFICANTLY DOWNREGULATED GENES

Biological Process	Combined Score	FDR	Overlap
organic acid catabolic process (GO:0016054)	41.00	1.50499E-08	35/200
carboxylic acid catabolic process (GO:0046395)	40.95	1.50499E-08	35/200
cellular amino acid metabolic process (GO:0006520)	40.58	3.70459E-08	51/421
small molecule catabolic process (GO:0044282)	40.28	3.70459E-08	39/261
dicarboxylic acid metabolic process (GO:0043648)	35.76	1.28014E-07	22/87
coenzyme metabolic process (GO:0006732)	29.63	2.15627E-06	30/196
alpha-amino acid catabolic process (GO:1901606)	29.56	1.35749E-06	21/92
cofactor metabolic process (GO:0051186)	28.76	3.83676E-06	34/255
cellular amino acid catabolic process (GO:0009063)	28.58	2.15627E-06	23/117
alpha-amino acid metabolic process (GO:1901605)	23.67	2.84938E-05	29/213

SIGNIFICANTLY UPREGULATED GENES

Biological Process	Combined Score	FDR	Overlap
response to endoplasmic reticulum stress (GO:0034976)	63.79	5.5045E-13	39/145
ER-nucleus signaling pathway (GO:0006984)	50.43	1.22345E-10	29/94
endoplasmic reticulum unfolded protein response (GO:0030968)	49.22	2.10104E-10	27/83
response to unfolded protein (GO:0006986)	49.21	2.54431E-10	33/135
cellular response to unfolded protein (GO:0034620)	48.68	2.54431E-10	27/86
response to topologically incorrect protein (GO:0035966)	47.27	6.88308E-10	33/143
cellular response to topologically incorrect protein (GO:0035967)	46.65	6.88308E-10	27/92
protein N-linked glycosylation via asparagine (GO:0018279)	34.18	1.75157E-07	24/96
peptidyl-asparagine modification (GO:0018196)	34.03	1.86284E-07	24/97
gene expression (GO:0010467)	33.91	4.40708E-07	70/672

Cellular Component	Combined Score	FDR	Overlap
organelle inner membrane (GO:0019866)	41.00	3.44957E-08	46/360
mitochondrial membrane (GO:0031966)	39.91	4.49838E-08	52/457
mitochondrial inner membrane (GO:0005743)	38.28	7.03569E-08	43/341
mitochondrion (GO:0005739)	20.34	0.00014029	88/1269
extracellular vesicular exosome (GO:0070062)	16.15	0.000578346	155/2717
very-low-density lipoprotein particle (GO:0034361)	9.70	0.015960442	6/20
oxidoreductase complex (GO:1990204)	9.67	0.010057058	13/88
triglyceride-rich lipoprotein particle (GO:0034385)	9.41	0.015960442	6/20
plasma lipoprotein particle (GO:0034358)	9.36	0.015960442	8/38
mitochondrial matrix (GO:0005759)	9.30	0.015158891	21/208

Cellular Component	Combined Score	FDR	Overlap
endoplasmic reticulum membrane (GO:0005789)	30.02	2.01305E-06	53/449
nucleoplasm (GO:0005654)	28.28	3.29534E-06	92/1051
integral component of endoplasmic reticulum membrane (GO:0030176)	12.42	0.003300267	16/94
nucleolus (GO:0005730)	12.21	0.003300267	113/1653
cytosol (GO:0005829)	11.66	0.003300267	160/2529
endoplasmic reticulum-Golgi intermediate compartment (GO:0005793)	9.24	0.014361872	10/47
integral component of organelle membrane (GO:0031301)	6.51	0.049290428	22/211
anchoring junction (GO:0070161)	6.34	0.057276314	35/419
adherens junction (GO:0005912)	6.27	0.057276314	34/405
late endosome (GO:0005770)	5.94	0.056552892	14/107

Molecular Function	Combined Score	FDR	Overlap
cofactor binding (GO:0048037)	33.40	1.50742E-06	36/266
pyridoxal phosphate binding (GO:0030170)	15.98	0.000932731	13/57
lyase activity (GO:0016829)	12.48	0.005557205	21/177
coenzyme binding (GO:0050662)	12.35	0.005557205	22/188
carbon-nitrogen lyase activity (GO:0016840)	9.28	0.022905778	5/10
NADH dehydrogenase (quinone) activity (GO:0050136)	8.95	0.022905778	9/46
NADH dehydrogenase (ubiquinone) activity (GO:0008137)	8.87	0.022905778	9/46
NADH dehydrogenase activity (GO:0003954)	8.78	0.022905778	9/46
lysophospholipid acyltransferase activity (GO:0042171)	8.22	0.030487068	5/12
flavin adenine dinucleotide binding (GO:0050660)	7.59	0.032683964	11/74

Molecular Function	Combined Score	FDR	Overlap
phosphate transmembrane transporter activity (GO:1901677)	6.21	0.119107898	6/20
nucleotide transmembrane transporter activity (GO:0015215)	5.85	0.119107898	5/15
intramolecular oxidoreductase activity, transposing S-S bonds (GO:0016864)	5.75	0.119107898	6/22
protein disulfide isomerase activity (GO:0003756)	5.67	0.119107898	6/22
low-density lipoprotein particle receptor binding (GO:0050750)	5.65	0.119107898	5/13
nucleotide-sugar transmembrane transporter activity (GO:0005338)	5.60	0.110256823	5/8
organophosphate ester transmembrane transporter activity (GO:0015605)	5.45	0.130610086	5/16
isomerase activity (GO:0016853)	5.15	0.110256823	19/159
unfolded protein binding (GO:0051082)	4.73	0.119107898	13/101
lipoprotein particle receptor binding (GO:0070325)	4.72	0.160729311	5/18

b

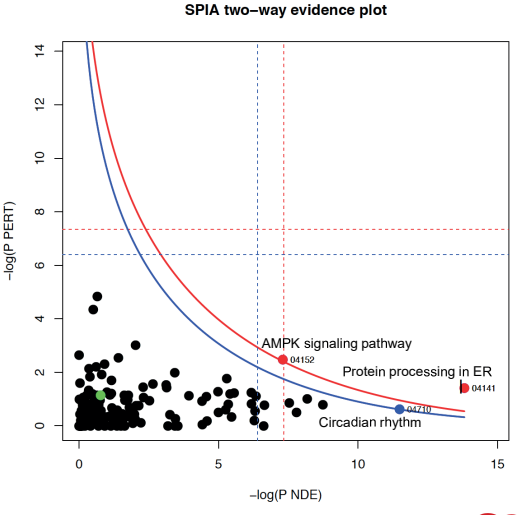

S2

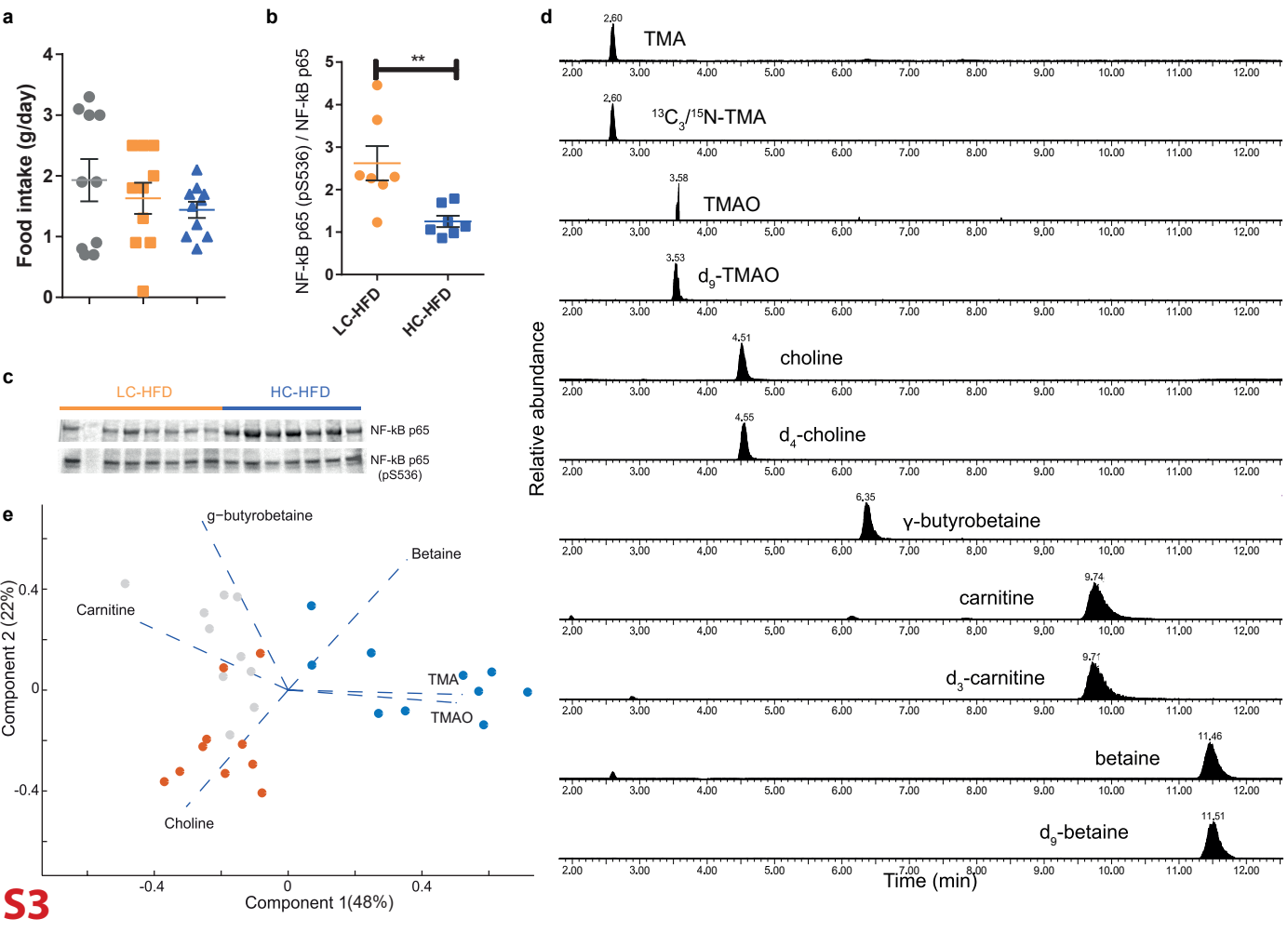
a
Food intake (g/day)
b
NF-kB p65 (pS536) / NF-kB p65
**
LC-HFD
HC-HFD
c
LC-HFD
HC-HFD
NF-kB p65
NF-kB p65 (pS536)
d
Relative abundance
TMA
13C3/15N-TMA
TMAO
d9-TMAO
choline
d4-choline
γ-butyrobetaine
carnitine
d3-carnitine
betaine
d9-betaine
Time (min)
e
g-butyrobetaine
Betaine
Carnitine
TMA
TMAO
Choline
Component 2 (22%)
Component 1(48%)
S3

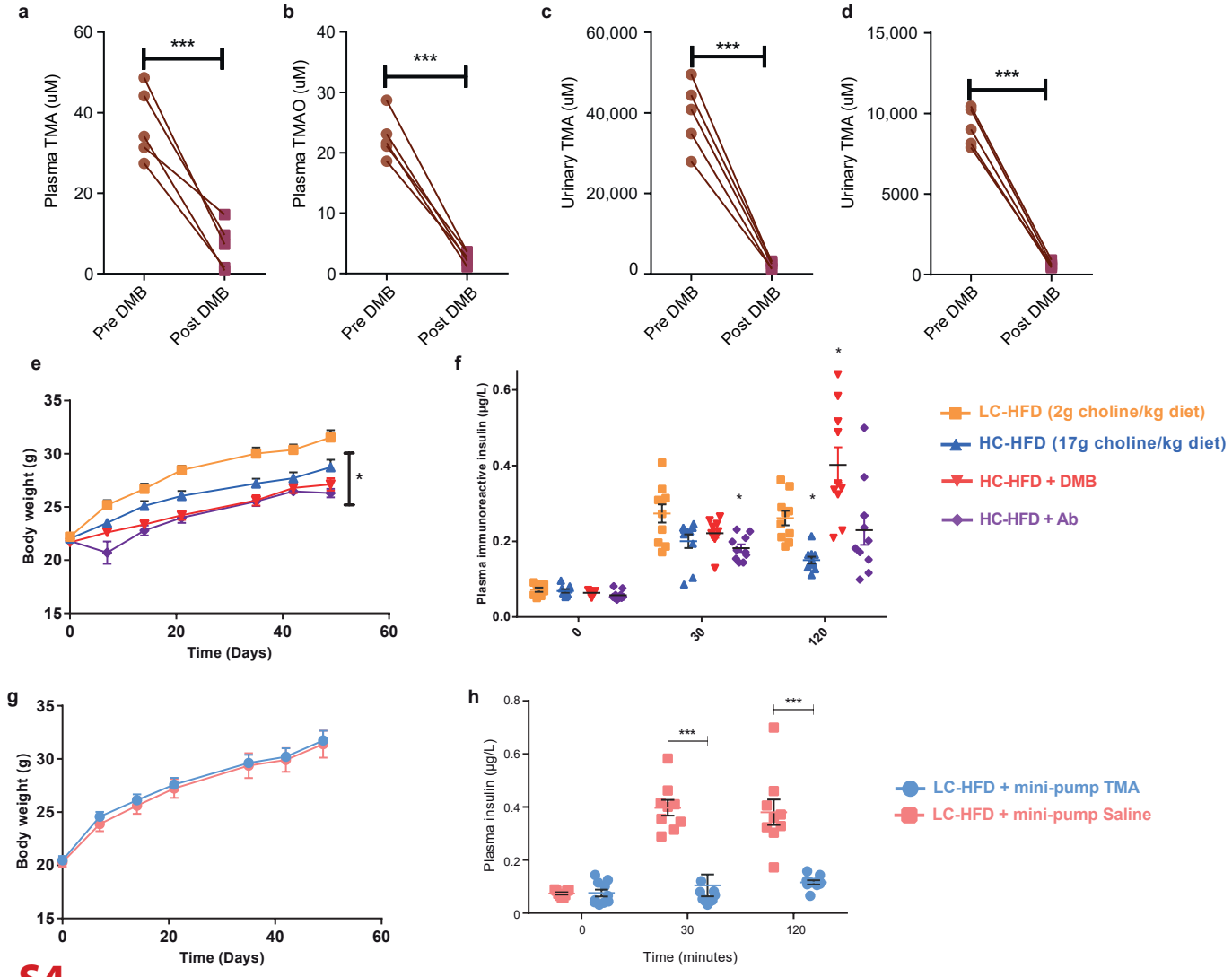
a
Plasma TMA (uM)
60
40
20
0
***
Pre DMB
Post DMB
b
Plasma TMAO (uM)
40
30
20
10
0
***
Pre DMB
Post DMB
c
Urinary TMA (uM)
60,000
40,000
20,000
0
***
Pre DMB
Post DMB
d
Urinary TMA (uM)
15,000
10,000
5000
0
***
Pre DMB
Post DMB
e
Body weight (g)
35
30
25
20
15
0
20
40
60
Time (Days)
*
f
Plasma immunoreactive insulin (µg/L)
0.6
0.4
0.2
0.0
0
30
120
*
*
*
LC-HFD (2g choline/kg diet)
HC-HFD (17g choline/kg diet)
HC-HFD + DMB
HC-HFD + Ab
g
Body weight (g)
35
30
25
20
15
0
20
40
60
Time (Days)
h
Plasma insulin (µg/L)
0.8
0.6
0.4
0.2
0
***
***
0
30
120
Time (minutes)
LC-HFD + mini-pump TMA
LC-HFD + mini-pump Saline

S4

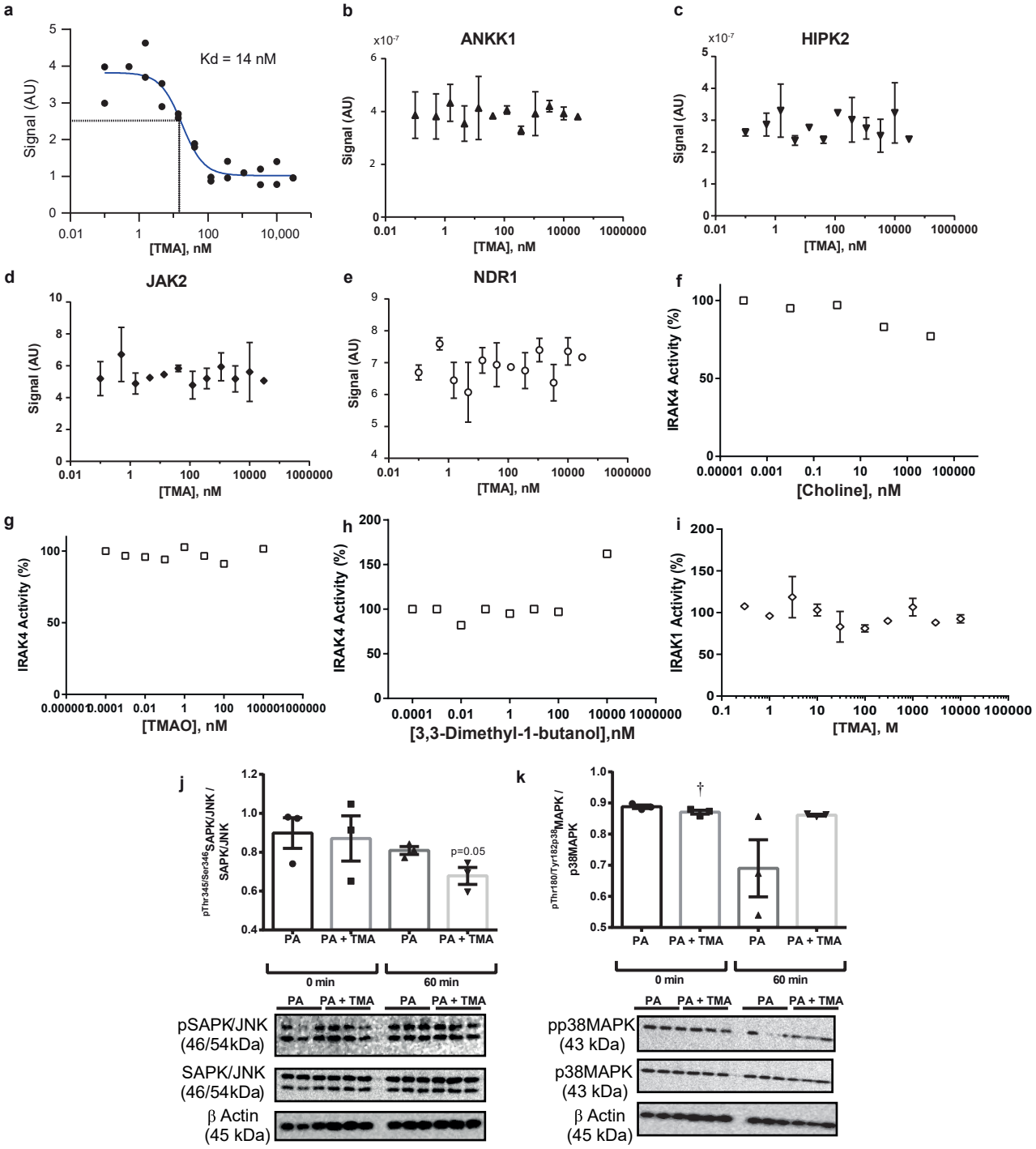
a
Kd = 14 nM
Signal (AU)
[TMA], nM
b
ANKK1
x10-7
Signal (AU)
[TMA], nM
c
HIPK2
x10-7
Signal (AU)
[TMA], nM
d
JAK2
Signal (AU)
[TMA], nM
e
NDR1
Signal (AU)
[TMA], nM
f
IRAK4 Activity (%)
[Choline], nM
g
IRAK4 Activity (%)
[TMAO], nM
h
IRAK4 Activity (%)
[3,3-Dimethyl-1-butanol],nM
i
IRAK1 Activity (%)
[TMA], M
j
pThr345/Ser346SAPK/JNK / SAPK/JNK
p=0.05
PA
PA + TMA
0 min
60 min
pSAPK/JNK (46/54kDa)
SAPK/JNK (46/54kDa)
β Actin (45 kDa)
k
pThr180/Tyr182p38MAPK / p38MAPK
†
pp38MAPK (43 kDa)
p38MAPK (43 kDa)
β Actin (45 kDa)

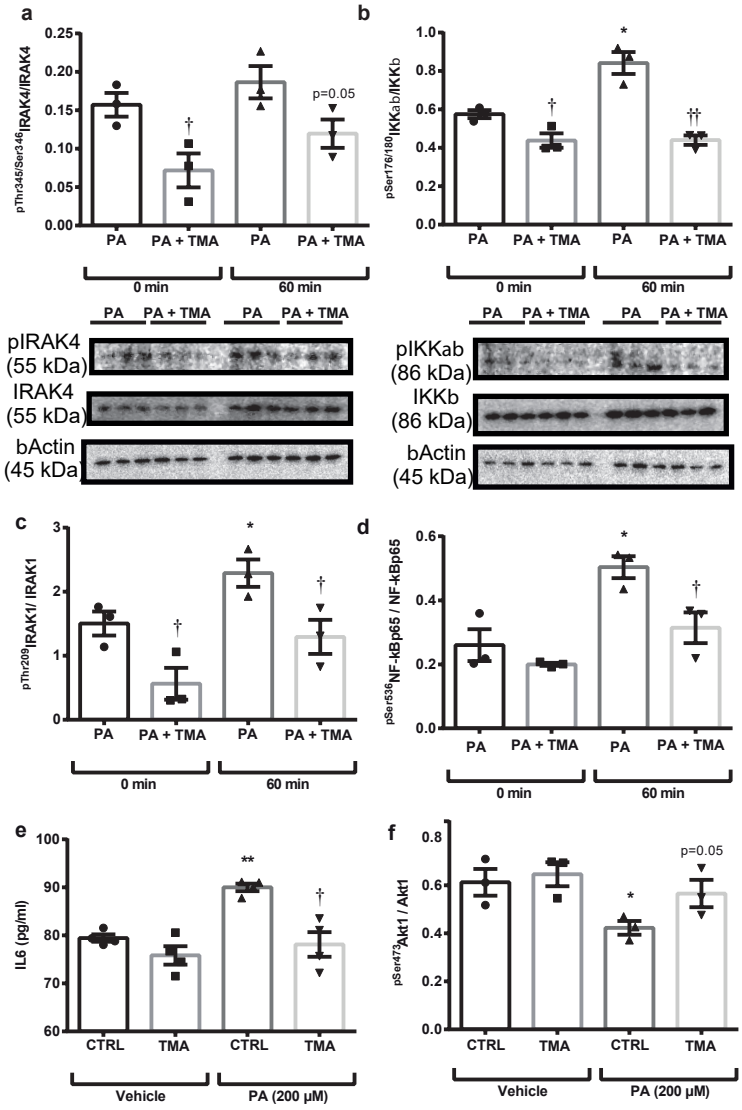
a
pThr345/Ser346IRAK4/IRAK4
0.25
0.20
0.15
0.10
0.05
0.00
p=0.05
PA
PA + TMA
PA
PA + TMA
0 min
60 min
PA
PA + TMA
PA
PA + TMA
pIRAK4
(55 kDa)
IRAK4
(55 kDa)
bActin
(45 kDa)
b
pSer176/180IKKa b/IKKb
1.0
0.8
0.6
0.4
0.2
0.0
PA
PA + TMA
PA
PA + TMA
0 min
60 min
PA
PA + TMA
PA
PA + TMA
pIKKab
(86 kDa)
IKKb
(86 kDa)
bActin
(45 kDa)
c
pThr209IRAK1/ IRAK1
3
2
1
0
PA
PA + TMA
PA
PA + TMA
0 min
60 min
d
pSer536NF-kBp65 / NF-kBp65
0.6
0.4
0.2
0.0
PA
PA + TMA
PA
PA + TMA
0 min
60 min
e
IL6 (pg/ml)
100
90
80
70
60
CTRL
TMA
CTRL
TMA
Vehicle
PA (200 µM)
f
pSer473Akt1 / Akt1
0.8
0.6
0.4
0.2
0.0
p=0.05
CTRL
TMA
CTRL
TMA
Vehicle
PA (200 µM)

S6

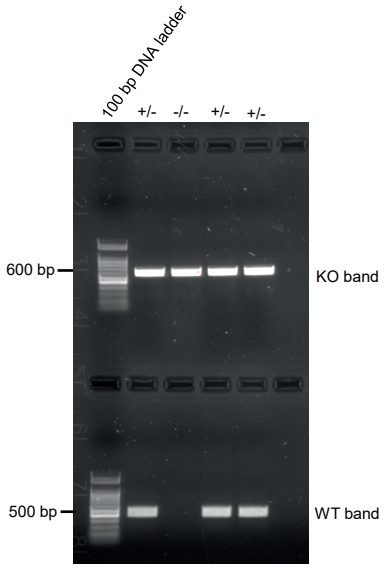
a
100 bp DNA ladder
+/-
-/-
+/-
+/-
600 bp
KO band
500 bp
WT band

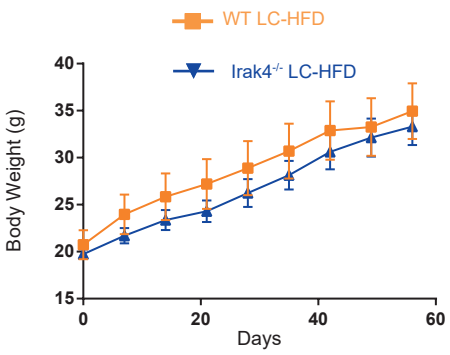
b
WT LC-HFD
Irak4-/- LC-HFD
Body Weight (g)
Days
40
35
30
25
20
15
0
20
40
60

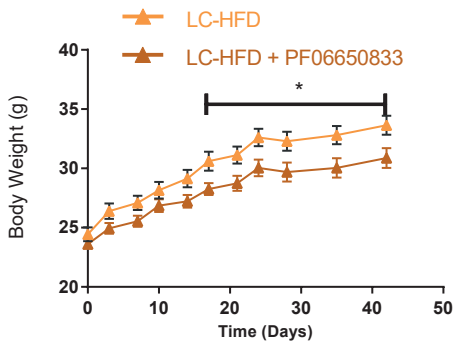
c
LC-HFD
LC-HFD + PF06650833
*
Body Weight (g)
Time (Days)
40
35
30
25
20
0
10
20
30
40
50